

Validation Report - MVIRI FCDR Release 1

DOI data 0-degree mission: 10.15770/EUM_SEC_CLM_0009
DOI data IODC 57-degree mission: 10.15770/EUM_SEC_CLM_0012
DOI data IODC 63-degree mission: 10.15770/EUM_SEC_CLM_0013

Doc.No. : EUM/OPS/DOC/18/990949
Issue : v3 e-signed
Date : 3 August 2020
WBS/DBS :

EUMETSAT
Eumetsat-Allee 1, D-64295 Darmstadt, Germany
Tel: +49 6151 807-7
Fax: +49 6151 807 555
<http://www.eumetsat.int>

Document Change Record

Version	Version Date (as on profile)	DCR* No. if applicable	Description of Changes
v1C	12 March 2019		First draft version
v1D	04 June 2019		Version ready for internal review
V2E	03 June 2020		Version after internal review
V3	3 August 2020		Final version

***DCR = Document Change Request**

Table of Contents

1	INTRODUCTION	8
1.1	Purpose and Scope	8
1.2	Structure of this Document.....	8
1.3	Acronyms	9
1.4	Definitions.....	10
2	BACKGROUND	10
2.1	MVIRI instrument	10
2.2	MVIRI data	11
2.3	Reprocessing algorithm	11
3	VALIDATION STRATEGY	12
3.1	Overall approach	12
3.2	Validation datasets	12
4	PRODUCT VALIDATION RESULTS.....	14
4.1	Time-series analysis	14
4.2	Comparison against superior reference.....	23
5	SUMMARY AND CONCLUSIONS	33
6	REFERENCES	35

Table of Figures

Figure 1: Theoretically expected time series of the reflectance derived from 6 Meteosat instruments at two reference sites using the (old) pre-launch measured SRFs and the (new) reconstructed, spectrally degrading SRFs. Grey shading indicates the combined standard uncertainty introduced by the SRFs.....	16
Figure 2: Reconstructed spectral response functions of Meteosat-2 to -7 plotted together with SCanning Imaging Absorption spectroMeter for Atmospheric CartograpHY (SCIAMACHY) spectra acquired during 2002 at three target sites. a) shows the spectra at the Algeria site, b) shows the spectra measured at the Nile-delta and the c) shows those measured at the Atlantic-1 site. SCIAMACHY spectra are plotted at in transparent black to better illustrate their spread. Spectra with strong cloud contamination were removed before plotting (see [RD 9] for details).	16
Figure 3: Recalibrated MVIRI clear sky reflectance time series and its uncertainties for the Algeria-3 site, calibrated with the reconstructed, in-flight characterised SRF.	17
Figure 4: Recalibrated MVIRI clear sky reflectance time series and its uncertainties for the Atlantic-1 site, calibrated with the reconstructed, in-flight characterised SRF.	18
Figure 5: Time series of recalibrated MVIRI clear-sky reflectance for the three sites Algeria-3 (top), Nile (middle), and Atlantic-1 (bottom), homogenised to the SRF of Meteosat-5.....	18
Figure 6: Anomalies of the homogenised clear-sky reflectance time series and their trends at three different sites. Anomalies are the deviation from the mean annual reflectance cycles. Bright grey shading denotes the uncertainties. Additional filtering for cloud contamination was applied as described in the text. Note that for the Atlantic site the periods with globally elevated aerosol loads due to volcanic eruptions (dark grey shading) are excluded from the stability analysis.	19
Figure 7: Homogenised time-series of operational IR channel radiances for the 0-degree measurements period. The homogenisation is performed using Meteosat-5 as the baseline satellite. The method to derive spectral band adjustment factors for the homogenisation is described in [RD 1] and [RD 6]. Each data point represents the average radiance of a slot (see text for details).	21
Figure 8: Homogenised time-series of recalibrated IR channel radiances for the 0-degree measurements period. The homogenisation is performed using Meteosat-5 as the baseline satellite. The method to derive spectral band adjustment factors for the homogenisation is described in RD 1. Each data point represents the average radiance of a slot (see text for details).	22
Figure 9: Homogenised time-series of operational WV channel radiances for the 0-degree measurements period. The homogenisation is performed using Meteosat-5 as the baseline satellite. The method to derive spectral band adjustment factors for the homogenisation is described in RD 7. Each data point represents the average radiance of a slot (see text for details).	22
Figure 10: Homogenised time-series of recalibrated WV channel radiances for the 0-degree measurements period. The homogenisation is performed using Meteosat-5 as the baseline satellite. The method to derive spectral band adjustment factors for the homogenisation is described in RD 7. Each data point represents the average radiance of a slot (see text for details).	23
Figure 11: Histogram of SEVIRI HRVIS reflectance plotted as reference together with the histograms of the operational MVIRI reflectance and the recalibrated MVIRI reflectance, as obtained from cloud-free Algeria-3 pixels at 12:00 UTC slots during March 2005. The MVIRI datasets are band adjusted to the SRF of the SEVIRI HRVIS band according to the given Spectral Band Adjustment Factors (SBAFs). The SBAFs are computed using the same set of SCIAMACHY spectra and the difference between both SBAFs is entirely due to the different shapes of the MVIRI SRFs in the operational and the recalibrated datasets.	25
Figure 12: Histogram of SEVIRI HRVIS reflectance plotted as reference together with the histograms of the operational MVIRI reflectance and the recalibrated MVIRI reflectance, as obtained from entirely cloud-covered pixels at 12:00 UTC slots during March 2005. Clouds are classified into high clouds (a), middle clouds (b) and low clouds (c). The MVIRI datasets were band adjusted to the SRF of the SEVIRI HRVIS band according to the given SBAFs. For each cloud-class the SBAFs for the operational dataset and for the recalibrated dataset are computed using the same set of SCIAMACHY spectra and the difference between both SBAFs is entirely due to the different shapes of the SRFs in the operational and recalibrated datasets.	26
Figure 13: Histogram of SEVIRI HRVIS reflectance plotted as reference together with the histograms of the operational MVIRI reflectance and the recalibrated MVIRI reflectance, as obtained from	

cloud-free Atlantic-1 pixels at 12:00 UTC slots during March 2005. The MVIRI datasets were band adjusted to the SRF of the SEVIRI HRVIS band according to the given SBAFs. The SBAFs are computed using the same set of SCIAMACHY spectra and the difference between both SBAFs is entirely due to the different shapes of the SRFs in the operational and the recalibrated datasets. 27

Figure 14: Locations of the areas considered for potentially finding ray-matched SCIAMACHY-MVIRI co-locations with Meteosat data from orbit positions 0° and IODC..... 27

Figure 15: Spectral characteristics of the collocation regions and of Algeria-3 collected during 10 days of February 2005. In order to emphasise on cloud-free surfaces a set of 10% of the darkest spectra was averaged for each region. For the Atlantic site also a set of the 10% brightest spectra was averaged to illustrate the spectral shape of cloudy observations. The grey shading indicates the standard deviation of each set. 28

Figure 16: Co-locations between SCIAMACHY and Meteosat-7 MVIRI reflectance for a) Atlantic-west, b) Atlantic-east and c) Kenya. Co-locations between SCIAMACHY and Meteosat-5 MVIRI reflectance are provided in d) for Somalia. Grey marks denote the dataset with the pre-launch SRF characterisation. Blue crosses denote the dataset using the reconstructed SRF. The co-locations are constrained to relative azimuth angles between the two instruments of 5°, to zenith angle differences of 15° and to acquisition time differences of 5 minutes. Only co-locations with a standard deviation of below 0.12 for MVIRI reflectance within a SCIAMACHY pixel are considered in order to reduce the matchup uncertainty for very heterogeneous scenes. Over the Atlantic, areas and the Somalian area co-locations were acquired from data collected during 2002–2006, whereas data collected during 2006–2010 were used for the co-locations over the Kenyan area. 29

Figure 17: Example schematic (not at the centre of the disc) of the MVIRI (2x2 red boxes) and SEVIRI (3x3 boxes with blue borders) pixel averaging kernels used for the comparison. 30

Figure 18: Results of the comparison of Meteosat-7 MVIRI operational (left) and recalibrated (right) against Meteosat-8 SEVIRI operational measurements for August 2004. The SEVIRI measurements are spectrally adjusted to MVIRI measurements as described in Section 4.1.2. 32

Figure 19: Comparison of operational (black), GSICS corrected (blue), and recalibrated (red) radiances for IR (top) and WV (bottom) channel measurements, see text for details. 33

Table of Tables

Table 1: Satellite names, mission names and nominal sub-satellite longitude in brackets, and operational years of the data that are validated in this report and made available in MVIRI FCDR Release 1. The FCDR includes observations from the 0-degree latitude and Indian Ocean Data Coverage (IODC) missions.	11
Table 2: Evaluation sites where band-adjusted (homogenised) time series were generated along with spectral characteristics and thresholds for the filtering of SCIAMACHY spectra according to Table 3.	15
Table 3: Tests for filtering SCIAMACHY spectra. Values for the thresholds are given in Table 2.	15
Table 4: Stability assessment of the harmonised and homogenised FCDR at three reference sites. .	20
Table 5: Spectral band adjustment factors (offset [$\text{mW}/\text{m}^2/\text{sr}/\text{cm}^{-1}$] and slope [unit less]) for the IR and WV channels to convert recalibrated radiances to homogenised radiances by taking Meteosat-5 as baseline.	20
Table 6: Unit conversion factor ($1000/\text{filter_integral}$) to convert radiances from $\text{W}/\text{m}^2/\text{sr}$ to $\text{mW}/\text{m}^2/\text{sr}/\text{cm}^{-1}$	21
Table 7: Geographical coordinates of the areas shown in Figure 14 as well as viewing zenith angle (VZA) and viewing azimuth angle (VAA) of SCIAMACHY observations considered for co-locations.	28

1 INTRODUCTION

1.1 Purpose and Scope

This document details the validation results for the first release of the Fundamental Climate Data Record (FCDR) of re-calibrated level-1.5 Infra-Red (IR), Water Vapour (WV), and Visible (VIS) channels radiance from the Meteosat Visible Infra-Red Imager (MVIRI) instrument onboard Meteosat First Generation (MFG) satellites, hereinafter referred to as MVIRI FCDR Release 1. Level-1.5 MVIRI data are projected to a predefined grid, with calibration information appended. The generation of the data record is the result of EUMETSAT's participation to two projects: the EU FP7 European Re-Analysis of the global CLIMate system (ERA-CLIM) 2 project [RD 3] and the EU H2020 Fidelity and uncertainty in climate data records from Earth Observations (FIDUCEO) [RD 4]. In the framework of ERA-CLIM2, the algorithms have been developed for the recalibration of infrared and water vapour observations from geostationary satellites. In the framework of FIDUCEO, which aimed to set new standards of accuracy and rigour in the generation of FCDRs with traceable uncertainty, the algorithms have been developed to recalibrate the visible channel observations from geostationary satellites.

The MVIRI FCDR Release 1 comprises MVIRI data from Meteosat-2, -3, -4, -5, -6 and -7 for the period 1982–2017, and provides a consistent record of recalibrated IR, WV, and VIS radiances, which can be used for climate monitoring and data assimilation. The data record can be regarded a FCDR, i.e., a long-term data record of calibrated and quality-controlled sensor data designed to allow the generation of homogeneous products that are accurate and stable enough for climate monitoring and data assimilation for re-analysis of the recent climate.

The reference data used to evaluate MVIRI FCDR Release 1 comprise Spinning Enhanced Visible and Infra-Red Imager (SEVIRI) datasets for IR, WV, and VIS channels, Global Space-based Inter-Calibration System (GSICS) corrected radiances for the IR and WV channels, and SCanning Imaging Absorption spectroMeter for Atmospheric CartographY (SCIAMACHY) measurements for the VIS channel.

1.2 Structure of this Document

Section 1	Purpose and scope of this validation report
Section 2	Background information
Section 3	Validation Strategy
Section 4	Product Validation Results
Section 5	Summary and Conclusions
Section 6	References

1.3 Acronyms

Acronym	Meaning
AIRS	Atmospheric Infrared Sounder
ATBD	Algorithm Theoretical Baseline Document
CGMS	Coordination Group for Meteorological Satellites
CODA	Common Data Access Toolbox
ECMWF	European Centre for Medium-Range Weather Forecasts
ERA-CLIM	European Re-Analysis of global Climate observations
ESA	European Space Agency
EU	European Union
EUMETSAT	European Organisation for the Exploitation of Meteorological Satellites
FCDR	Fundamental Climate Data Record
FIDUCEO	Fidelity and uncertainty in climate data records from Earth Observations
FP7	7th Framework programme
GSICS	Global Space-based Inter-Calibration System
HRVIS	High-Resolution VISible
IASI	Infrared Atmospheric Sounding Interferometer
IODC	Indian Ocean Data Coverage
IR	Infra-Red
MFG	Meteosat First Generation
MSG	Meteosat Second Generation
MVIRI	Meteosat Visible Infra-Red Imager
NeDT	Noise Equivalent Differential Temperature
NWP	Numerical Weather Prediction
RicalPy	Re-calibration and Inter-calibration Software
RTM	Radiative Transfer Model
SBAF	Spectral Band Adjustment Factor
SCIAMACHY	SCanning Imaging Absorption spectroMeter for Atmospheric CartographY
SEVIRI	Spinning Enhanced Visible and Infra-Red Imager
SNO	Simultaneous Nadir Overpass
SRF	Spectral Response Function
SSCC	SEVIRI Solar Channel Calibration
SWIR	ShortWave Infra-Red
UV	UltraViolet
VIS	Visible
VZA	Viewing Zenith Angle
WMO	World Meteorological Organisation
WV	Water Vapour
ZDM	Zero Degree Mission

1.4 Definitions

The following definitions are used throughout the document.

Products types:

- Fundamental Climate Data Record [RD 5] - is a well-characterised, long-term data record, usually involving a series of instruments, with potentially changing measurement approaches, but with overlaps and calibrations sufficient to allow the generation of products that are accurate and stable, in both space and time, to support climate applications. FCDRs are typically calibrated radiances, backscatter of active instruments, or radio occultation bending angles. FCDRs also include the ancillary data used to calibrate them.
- Monitored sensor – refers to the sensor that is subject to (re)calibration.
- Reference sensor – refers to the sensor, preferably with superior quality, which is used as (re)calibration reference.

Harmonisation and Homogenisation [RD 1]:

- Harmonisation of a dataset is equivalent to a consistent recalibration of a series of instruments. The observations represent the physics of each instrument, in particular the spectral weighting of the incoming light by the spectral response functions. As the spectral response functions differ for instruments, jumps due to instrument switches are expected.
- Homogenisation of a dataset uses a-priori knowledge about the spectrum of the observed target to adjust the differences between spectral response functions. For the visible band homogenisation is particularly challenging: the band adjustment functions between two instruments remain constant for different brightness levels, but they lose validity as soon as the shape of the target spectrum changes. This can happen e.g. due to cloud contamination or natural seasonality. Jumps due to instrument switches are not expected.

2 BACKGROUND

In this chapter, background information is provided on the MVIRI instrument, on the data that have been reprocessed and on the algorithms that have been used for the reprocessing. In order to improve the readability of the document, the reprocessing procedure is briefly summarized.

2.1 MVIRI instrument

The MVIRI instrument was operated onboard seven MFG satellites during the years 1977 – 2017. MVIRI was equipped with three channels:

- one broadband solar channel (central wavelength 0.7 μm ; spectral interval 0.4 -1.2 μm);
- one infra-red channel (central wavelength 10.8 μm ; spectral interval 10.5–12.5 μm ; pre-launch specified Noise Equivalent Differential Temperature (NeDT) 0.5K@250K);
- one water vapour channel (central wavelength 6.4 μm ; spectral interval 5.7–7.1 μm ; pre-launch specified NeDT 1.0K@250K).

The nadir spatial resolution of MVIRI was 2.25 \times 2.25 km² for the visible channel, and 4.50 \times 4.50 km² for the infra-red and the water vapour channels.

2.2 MVIRI data

Table 1 shows for each satellite the orbital position and the main years of operation. Please note that an archive of Meteosat-1 data has only been recently rescued for December 1978 to November 1979. Those data need much more preparatory work before being available for any FCDR generation. In addition, data from the Atlantic Data Coverage and EXtended Atlantic Data Coverage have not been used for this FCDR release. These data may be included in later releases of the FCDR.

Table 1: Satellite names, mission names and nominal sub-satellite longitude in brackets, and operational years of the data that are validated in this report and made available in MVIRI FCDR Release 1. The FCDR includes observations from the 0-degree latitude and Indian Ocean Data Coverage (IODC) missions.

Satellite	Orbital Position	Main Operational Years	# of years
Meteosat-1	0-degree (0°)	1977-1979	2
Meteosat-2	0-degree (0°)	1981-1988	7
Meteosat-3	0-degree (0°)	1988-1991	3
Meteosat-3	ADC (-50°)	1991-1993	2
Meteosat-3	XADC (-75°)	1993-1995	2
Meteosat-4	0-degree (0°)	1989-1994	5
Meteosat-5	0-degree (0°)	1991-1997	7
Meteosat-5	IODC (63°)	1998-2007	9
Meteosat-6	0-degree (0°)	1996-1998	2
Meteosat-6	IODC (67°)	2007-2009	2
Meteosat-7	0-degree (0°)	1998-2007	9
Meteosat-7	IODC (57°)	2007-2017	10

2.3 Reprocessing algorithm

The MVIRI FCDR Release 1 has been generated based on the physical methods described in [RD 1]. The algorithm merges two calibration chains. Firstly, the IR recalibration algorithm, which is used for generating the re-calibration coefficients for the MVIRI IR and WV channels [RD 1] and [RD 6]. Secondly, the Visible channel algorithm (a modified version of the Spinning Enhanced Visible and Infra-Red Imager (SEVIRI) Solar Channel Calibration (SSCC) algorithm [RD 10]) for automated vicarious calibration, which is used for generating the re-calibration coefficients for the MVIRI VIS channel [RD 1][RD 7], [RD 8], and [RD 9].

The IR recalibration algorithm adopts a Simultaneous Nadir Overpass (SNO) approach for recalibrating IR and WV channel radiance measurements from MVIRI, using superior quality measurements from infra-red sounders on polar orbiting satellites as a reference. The IR recalibration algorithm follows the following sequence: 1) selecting reference instruments, 2) co-locating monitored and reference measurements, 3) adjusting reference measurements for spectral band differences, 4) filtering the co-locations based on pre-defined criteria, and 5) computing of re-calibration coefficients and associated uncertainties.

The SSCC algorithm adopts a vicarious calibration approach for recalibrating VIS channel reflectance derived from MVIRI data. The principle of the algorithm is based on a comparison of observed and simulated radiances for a set of predefined desert and ocean targets. A Radiative Transfer Model (RTM) is used to simulate the radiance over the identified targets, taking into account atmospheric properties, satellite and solar viewing geometries, bi-

directional reflectance distribution function of the target, and the spectral response function of the instrument including its spectral aging. The SSCC algorithm follows the following sequence: 1) calculating calibration coefficients for each target and for each time slot; 2) averaging calibration coefficients for each target over all time slots and assigning a weight based on quality; 3) deriving calibration coefficients and associated errors for each target; 4) accepting or rejecting the calibration coefficients of the two types of targets. Finally, the algorithm also computes uncertainties arising from various error sources in the measurement and calibration processes.

3 VALIDATION STRATEGY

This chapter presents the validation strategy of the FCDR and the validation data sets that are used.

3.1 Overall approach

The scientific validation of the MVIRI FCDR Release 1, presented in this validation report involved the following analyses:

- **Time-series analysis** – this analysis aims to demonstrate the temporal consistency across different satellites before and after the recalibration. In order to do this for the visible channel measurements, the time series have to be extracted for specific locations/sites where a-priori knowledge about the expected spectrum is available. This knowledge is obtained by exploiting SCIAMACHY spectra; after dataset homogenisation, the analysis of the time series allows to quantitatively validate the consistency and the stability of the calibration over time. For the IR/WV channels, IASI data are used to compute band adjustment factors to perform inter-satellite homogenisation.
- **Comparison against superior reference** – the comparison against a superior reference is performed in order to give an indication of whether the trueness of the dataset has improved. Therefore, the data are compared with SEVIRI measurements onboard Meteosat Second Generation (MSG) and with the hyperspectral measurements from SCIAMACHY. For IR/WV channel, the recalibrated radiances are also compared against the radiances corrected by GSICS methodology [RD 21], which used IASI data as reference measurements. This comparison shall be considered more as a sanity check of the recalibration methodology than a real comparison against superior measurements because our recalibrated methods only has subtle differences with GSICS methods when both of them uses IASI data as reference measurements. Ideally, the recalibrated radiances shall be compared against superior measurements from hyperspectral instruments such as IASI and AIRS, but we are unable to do this because these measurements have already been used for computing the recalibration coefficients.

3.2 Validation datasets

This section summarises the data sets that are used for the validation of the MVIRI FCDR Release 1.

3.2.1 SCIAMACHY

SCIAMACHY was a scanning nadir and limb spectrometer covering the ultraviolet (UV) through visible to shortwave infra-red (SWIR) spectral range. SCIAMACHY was a joint development of Germany, the Netherlands and Belgium and was launched in February 2002 onboard the ENVISAT platform operated by the European Space Agency (ESA) [RD 29]. About 10 years after launch, on April the 8th 2012, ESA lost contact with the ENVISAT satellite. ENVISAT was a sun-synchronised polar orbiting satellite with a local equator crossing time of 10:00 AM and an orbital period of about 100 minutes. SCIAMACHY performed nadir and limb measurements. In limb mode, the instrument observed a certain volume of the atmosphere about 7 minutes before it was observed in nadir mode. The orbit swath is 960 km wide. The wavelength range covered by SCIAMACHY is 240–2380 nm in eight spectral channels with a spectral resolution between 0.2–1.5 nm. Light that entered the instrument was dispersed using an assembly of prisms and holographic diffraction gratings onto the arrays of 1024 detectors per channel. While reticon photodiodes were used for the five UV-VIS channels, the three SWIR channels were equipped with Indium Gallium Arsenide detectors [RD 22]. The 1024 detectors were sub-divided into clusters that are useful for trace-gas retrieval. As each detector, after the dispersion and bending of the incoming light beam, represented a unique wavelength, the clusters corresponded to wavelength regions. For each of the 56 clusters the integration time could be varied, resulting in various spatial resolutions. This allowed a higher spatial resolution for the most important spectral regions and longer integration times where needed. In order to cover the entire measured spectrum, the measurements of all clusters have to be integrated into the broadest pixel size. Global coverage (in nadir mode) is achieved in six days [RD 23]. Originally designed for studying atmospheric chemistry and aerosols [RD 24], the instrument has proven to be very useful for the cross-calibration, band adjustment and validation of other satellites in numerous studies [RD 14], [RD 25], [RD 26], [RD 27] and [RD 28]. The Level 1 dataset has undergone several recalibration campaigns. The latest version (V8) of the Level 1b dataset contains all calibration parameters described in [RD 30]. It can be converted into calibrated Level 1c using the Common data access (CODA) toolbox software package [RD 31].

SCIAMACHY measurements can be considered as superior to MVIRI measurements because of several reasons - it has an on-board calibration device, stricter noise specifications, finer digitisation (16bit), and the hyperspectral nature of the measurements avoids uncertainties associated with the position and shape of spectral response functions of broadband radiometers such as MVIRI.

3.2.2 SEVIRI

SEVIRI is a radiometer onboard a series of four MSG satellites that are operated by EUMETSAT in geostationary orbit. In 2002, the first MSG satellite (Meteosat-8) was launched. Similar to the MFG satellites, the MSG satellites are spin-stabilised. The SEVIRI instrument operates 12 channels simultaneously. Three of its channels are at visible and near infra-red wavelengths between 0.6 and 1.6 μm , eight channels are at infra-red wavelengths between 3.8 and 14 μm and one channel is a high-resolution visible (HRVIS) channel. For this study, the HRVIS channel is of relevance due to its broad spectral coverage being comparable to the MVIRI VIS channel. As for MVIRI VIS, the detectors employed are silicon photodiodes. In contrast to the latter, however, not only two detectors are operated simultaneously, but an array of 9 detectors. With this setup, the HRVIS channel acquires 9 scanlines during each revolution of the satellite. In this way a full-disc earth scan can be performed every 15 minutes, much faster than with MVIRI. During the period 2004–2006, Meteosat-8 was operated at a

sub-satellite longitude close to Meteosat-7. This period therefore is predestined for useful comparisons between SEVIRI and MVIRI. The characteristic of the four solar channels are summarised in Table 2 according to the Meteosat-8 (MSG1) commissioning report [RD 32].

SEVIRI measurements can be considered superior to MVIRI measurements because of their better pre-launch characterisation and due to the availability of onboard calibration targets for the longwave channels.

3.2.3 GSICS Corrections

Sponsored by the World Meteorological Organization (WMO) and the Coordination Group for Meteorological Satellites (CGMS), the Global Space-based Inter-Calibration System ([RD 15] and [RD 21]) aims to inter-calibrate a diverse range of satellite instruments to produce corrections ensuring their data are consistent, allowing them to be used to produce globally homogeneous products for environmental monitoring. Although these instruments operate on different technologies for different applications, their inter-calibration can be based on common principles: Observations are co-located, transformed, compared and analysed to produce calibration correction functions, transforming the observations to common references. The details of this methodology are given in [RD 21]. GSICS corrections are available for Meteosat-7 since June 2008 until the end of the satellite's lifetime (April 2017). The GSICS corrections are only used as a sanity check for recalibrated IR and WV channel radiances as explained in Section 3.1.

4 PRODUCT VALIDATION RESULTS

In this chapter, the results of the product validation are presented. The structure follows that of the high-level validation approach described above. The VIS channel and the WV/IR channels are validated separately. A proper validation of the VIS channel data is not straightforward, because the channel is spectrally very broad, because the shapes of the spectral response functions (SRF) varies between instruments and because each SRF is subject to spectral degradation with time. Moreover, the differences of the reflectance spectra at different sites emphasise different parts of the spectral response functions (Figure 2). Differences between measurements of different instruments are therefore variable at pixel level.

4.1 Time-series analysis

4.1.1 Visible channel

The calibration of the visible channel of the MVIRI instrument relies heavily on the spectral response function (SRF) of the detectors. Despite using roughly the same instrument model, small changes of the silicon detectors and telescope that were employed on the fleet of the Meteosat First Generation spacecraft have resulted in different shapes of the SRF. Additionally, the requirements regarding the accuracy, the precision and the spectral resolution of the pre-launch characterisation have changed over time. This has resulted in reported shortcomings of the available MVIRI data [RD 11], [RD 12] and [RD 13].

In the course of the generation of the presented FCDR, the SRFs of all MVIRI instruments have been reconstructed, taking into account spectral degradation [RD 7] and [RD 8]. The expected impact of the reconstructed SRFs against the pre-launch SRFs is demonstrated in Figure 1. The time series are computed by convoluting the pre-launch and reconstructed SRFs with representative mean spectra at two reference sites: a desert site (Algeria3) and a site in the Atlantic. The mean spectra for those sites were obtained from SCIAMACHY measurements

(Figure 2). The faster degradation of the reconstructed SRFs in the blue part of the spectrum results in increasing (decreasing) reflectance values at the Algeria-3 (Atlantic-1) site (see Table 2) over the lifetime of each satellite. An exception is Meteosat-6, where this pattern is inverted. This could be due to the very short time period available which reduces the quality of the SRF reconstruction.

Table 2: Evaluation sites where band-adjusted (homogenised) time series were generated along with spectral characteristics and thresholds for the filtering of SCIAMACHY spectra according to Table 3.

Site	Land Cover Type	Dominant Spectral Contribution	Central Latitude	Central Longitude	Size of Box	thr_1	thr_2	thr_3	thr_4
Algeria-3	Desert	Red	30.32	7.66	$2^\circ \times 2^\circ$	0.47	0.38	15	0.5
Nile	Agricultural land	Green	30.5	31.25	$0.5^\circ \times 0.5^\circ$	0.35	0.35	20	0.03
Atlantic-1	Sea	Blue	-22.5	9.5	$2^\circ \times 2^\circ$	0.02	0.053	5	0.02

Table 3: Tests for filtering SCIAMACHY spectra. Values for the thresholds are given in Table 2.

Test	Condition	Rationale
1	$\frac{\overline{L}_s(1120nm : 1150nm)}{\overline{L}_s(317nm : 350nm)} < thr_1$	Cloud rejection: Radiance between 1120nm and 1150nm is subject of H ₂ O absorption. Clouds reduce the H ₂ O absorption path through the atmosphere and therefore increase this ratio.
2	$\int_{\lambda} R_s(\lambda)\phi(\lambda)d\lambda < thr_2$	Cloud rejection: The reflectance is convoluted with the spectral response function of the instrument that is the reference for the band-adjustment. Cloud contamination increases the convoluted reflectance in the VIS range.
3	$ \beta_{scia} - \beta_{mviri} < thr_3$	Only SCIAMACHY observations with viewing geometries that are comparable to MVIRI geometries are considered. Here β denotes the scattering angles of both SCIAMACHY and MVIRI.
4	$\sigma(R_M) < thr_3$	Only SCIAMACHY observations with low scene heterogeneity are considered in order to avoid inconsistencies of the band adjustment due to remaining clouds or unwanted surface features.

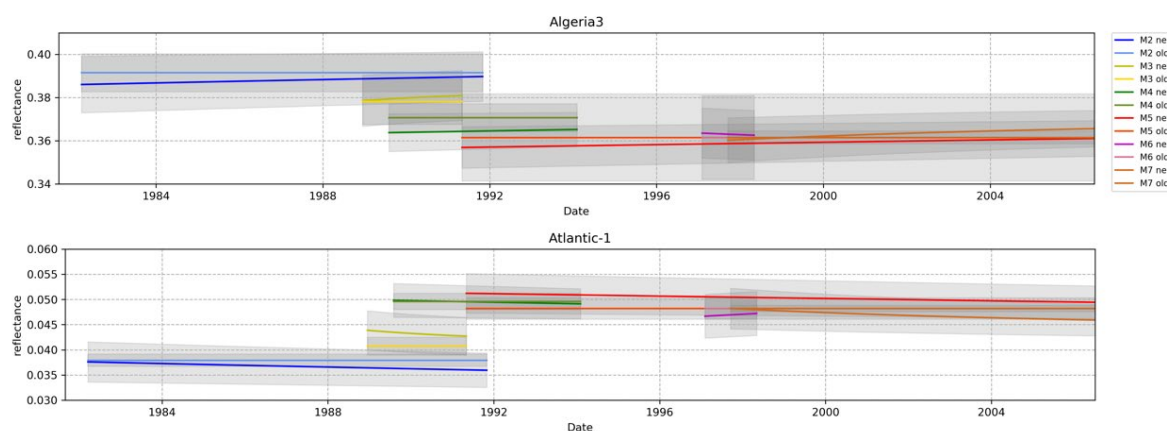


Figure 1: Theoretically expected time series of the reflectance derived from 6 Meteosat instruments at two reference sites using the (old) pre-launch measured SRFs and the (new) reconstructed, spectrally degrading SRFs. Grey shading indicates the combined standard uncertainty introduced by the SRFs.

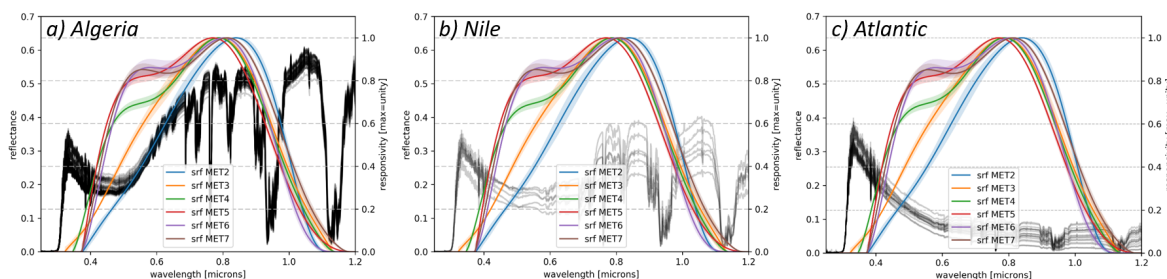


Figure 2: Reconstructed spectral response functions of Meteosat-2 to -7 plotted together with SCanning Imaging Absorption spectroMeter for Atmospheric Cartography (SCIAMACHY) spectra acquired during 2002 at three target sites. a) shows the spectra at the Algeria site, b) shows the spectra measured at the Nile-delta and the c) shows those measured at the Atlantic-1 site. SCIAMACHY spectra are plotted in transparent black to better illustrate their spread. Spectra with strong cloud contamination were removed before plotting (see [RD 9] for details).

Harmonised time series

The observed time series of clear-sky reflectance extracted from the harmonised MVIRI VIS FCDR match well with the above-described expectations. The most striking features are the jumps between the different sensors. Particularly Meteosat-2 and -3 deviate from the other satellites. At the Algeria-3 target site, with its dominant spectral contribution in the red, the clear-sky reflectance values from Meteosat-2 and -3 are brighter than those of Meteosat-4,-5,-6, and -7 (Figure 3). At the Atlantic-1 target site, with its dominant spectral contribution in the blue, the clear-sky reflectance values from Meteosat-2 and -3 are darker than those from the other satellites (Figure 4). The observed differences can be explained by the differences between the SRFs of Meteosat-2 and -3 and the other satellites (see Figure 1 and Figure 2). From Figure 2 it can be seen that the spectral response of Meteosat-2 and -3 is much weaker between 0.4 and 0.6 μm compared to the spectral response of Meteosat-4,-5,-6,-7. Therefore, the clear-sky reflectance of Meteosat-2 and -3 measured at Atlantic-1, which reflects most at wavelengths smaller than 0.6 μm must be lower than from the other satellites. The opposite

applies for Algeria-3, which reflects most at wavelengths larger than $0.6 \mu\text{m}$. For the green Nile delta (not shown) no noticeable jumps are present.

Figure 3 also show time series of the independent and structured uncertainties determined with the methods laid out in [RD 1]. The uncertainty for data from the Meteosat-2 satellite is small because of the coarse digitisation. While the coarse digitisation increases the digitisation noise (see equation 10 in [RD 1]), this is compensated by the fact that the noise of the sensor voltage before reaching the analogue-to-digital converter has to be much larger in order to trigger any noise in the digitised signal. The seesaw-like pattern of the Meteosat-2 uncertainties may be attributed to the annual cycle of the instrument temperature. This cycle is a result of the satellite being heated by the sun from different angles over the year and it is recorded in the instrument telemetry data. Highest instrument temperatures occur during the winter months and highest diurnal amplitudes of the temperatures occur during the eclipse seasons in spring and autumn. Higher instrument temperatures lead to an increase of the noise of the onboard electronics and increase the differences of the sensitivities of the two detectors. In this way, the variations in instrument temperature affect the independent and the structured uncertainty. The uncertainty of Meteosat-2 data has been reduced as compared to what was reported in [RD 9]. This was achieved by an improved flagging of lines containing no data. For Meteosat-3 the improved flagging has not been applied.

The influence of instrument temperature variations is smaller for the newer satellites (Meteosat-4, -5, -6 and -7) because of enhanced sun protection. The bulging pattern of the independent uncertainty of Meteosat-7 can be attributed to a very different noise level of the two detectors on this satellite. This increases the uncertainty of the signal when combined for the two detectors. During June–August, the difference in noise level between the two detectors is mitigated by the temperature dependent switches of the Analog-to-Digital converters of the two detection chains [RD 33]. The bulging pattern is only visible at the bright Algeria site, while it is not visible at the dark Atlantic site that shows higher uncertainty because the measurement of the much smaller reflectance is very sensitive to instrument noise.

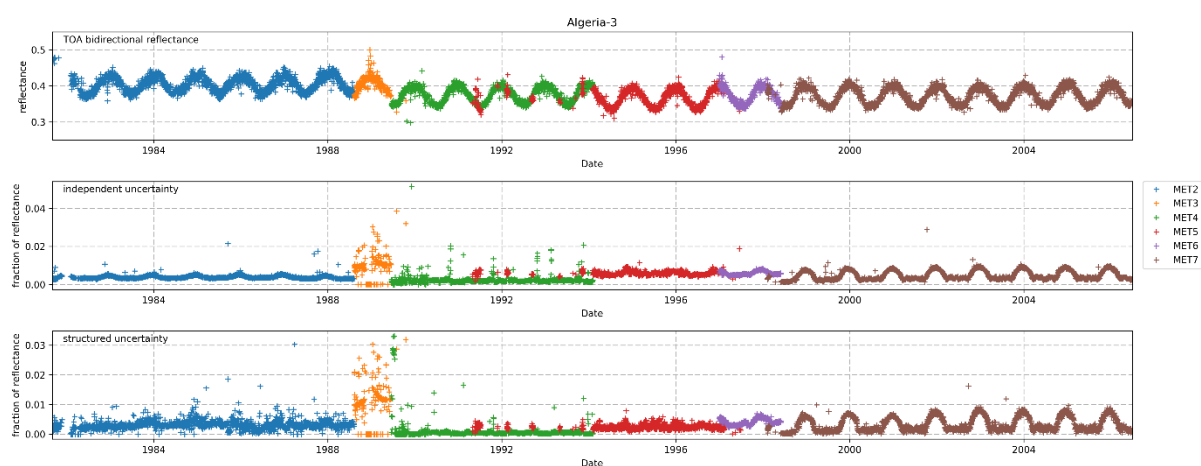


Figure 3: Recalibrated MVIRI clear sky reflectance time series and its uncertainties for the Algeria-3 site, calibrated with the reconstructed, in-flight characterised SRF.

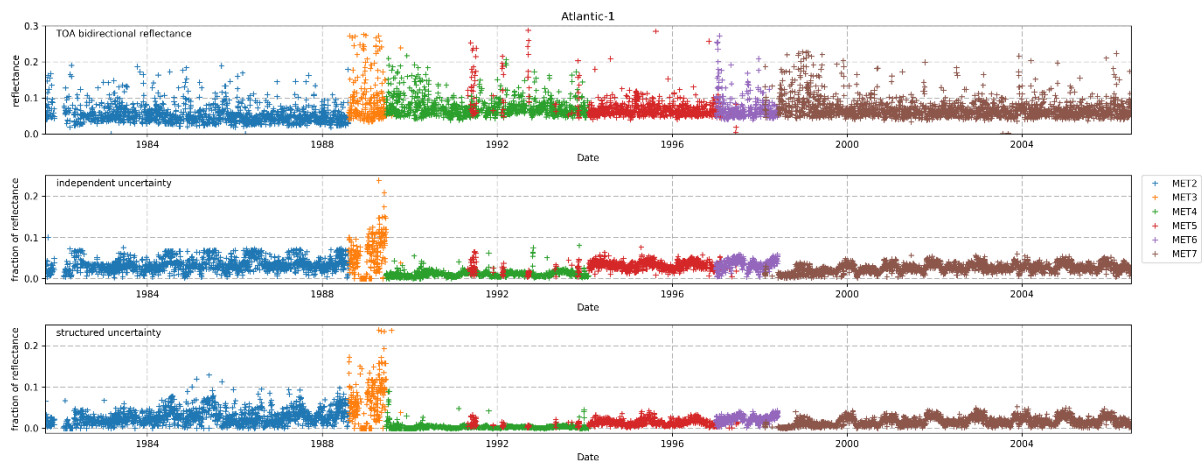


Figure 4: Recalibrated MVIRI clear sky reflectance time series and its uncertainties for the Atlantic-1 site, calibrated with the reconstructed, in-flight characterised SRF.

Homogenised time series

The recalibrated (harmonised) FCDR with reconstructed SRFs does not hide the SRF degradation at any target type: The jumps and trends of the BRF that are expected from the changing SRFs are clearly visible in the time series (Figure 7 and Figure 8). In order to evaluate the consistency of the assumption, that the jumps and trends in the recalibrated dataset can indeed be explained by the SRF shapes, the time series are homogenised (Figure 5). For the homogenisation SCIAMACHY data are used to infer the spectral reflectance of the surface and to compute target-specific band-adjustment functions [RD 9]. The disappearance of jumps and trends in the homogenised time series for all target sites is a clear indicator for a successful characterisation of the SRFs in the FCDR.

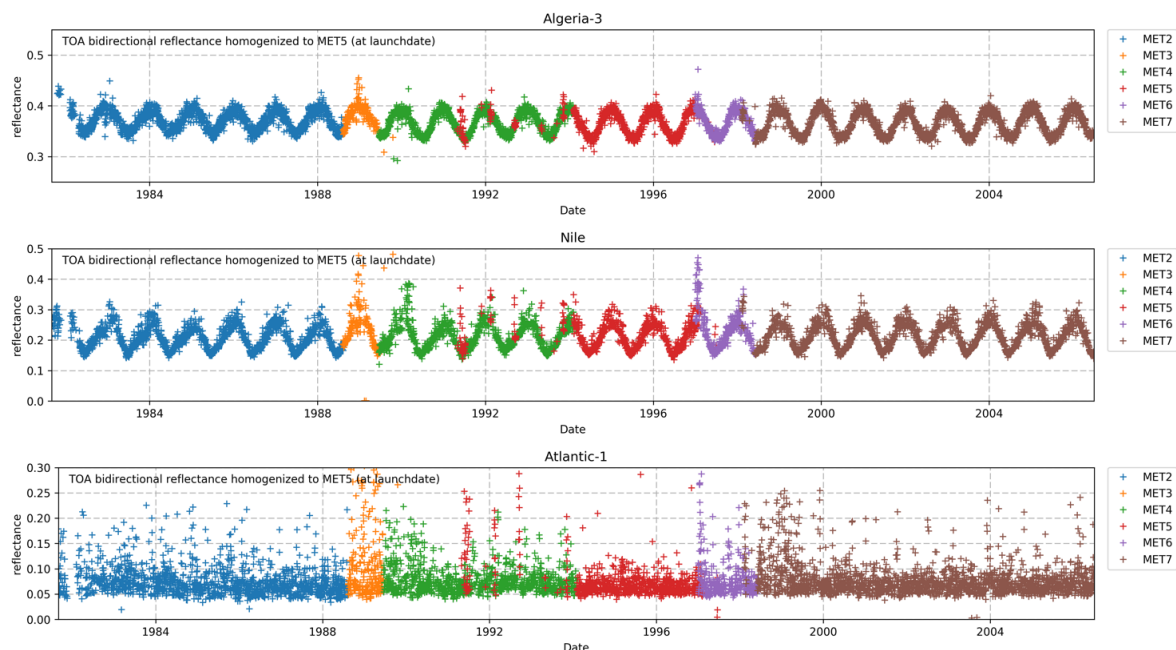


Figure 5: Time series of recalibrated MVIRI clear-sky reflectance for the three sites Algeria-3 (top), Nile (middle), and Atlantic-1 (bottom), homogenised to the SRF of Meteosat-5.

Outliers at the Algeria site only occur for the short duration of the Meteosat-3 coverage during winter, pointing to issues of the cloud mask [RD 35]. Cloud contamination at the Nile delta is generally higher. Furthermore, impacts of human activities may occur at this site. This leads to a generally higher probability for variability, and that is confirmed by data. The clear-sky reflectance above the Atlantic are, as expected, around 0.05. The high spread of the observed values at this site again points to not detected clouds. In order to exclude the variable performance of the cloud mask from the stability evaluation of the dataset, we implemented a consistent filtering across all satellites as an intermediate step (see [RD 9]). The filter computes the 25th percentile from a rolling kernel of 30 days around each reflectance measurement. Measurements that are brighter than this value are rejected in order to display only measurements that are certainly cloud free. After applying this filtering the anomalies of the clear-sky reflectance time series (Figure 6) have been evaluated on their decadal stability. Over pseudo-invariant calibration targets, one would not expect the signal to vary significantly over time. The results indeed reveal very stable behaviour for Algeria-3 and for the Nile delta sites with trends around -0.6% and 1.7 % per decade in reflectance (see Table 4). Results for the Atlantic-1 site are worse with around 7.5% decadal change in reflectance. The main contribution to this change comes from the too dark values of Meteosat-2 (see Figure 6). Since the homogenisation has removed the effects of the different SRFs, this finding indicates a potential overestimation of the Meteosat-2 SRF in the blue region of the spectrum.

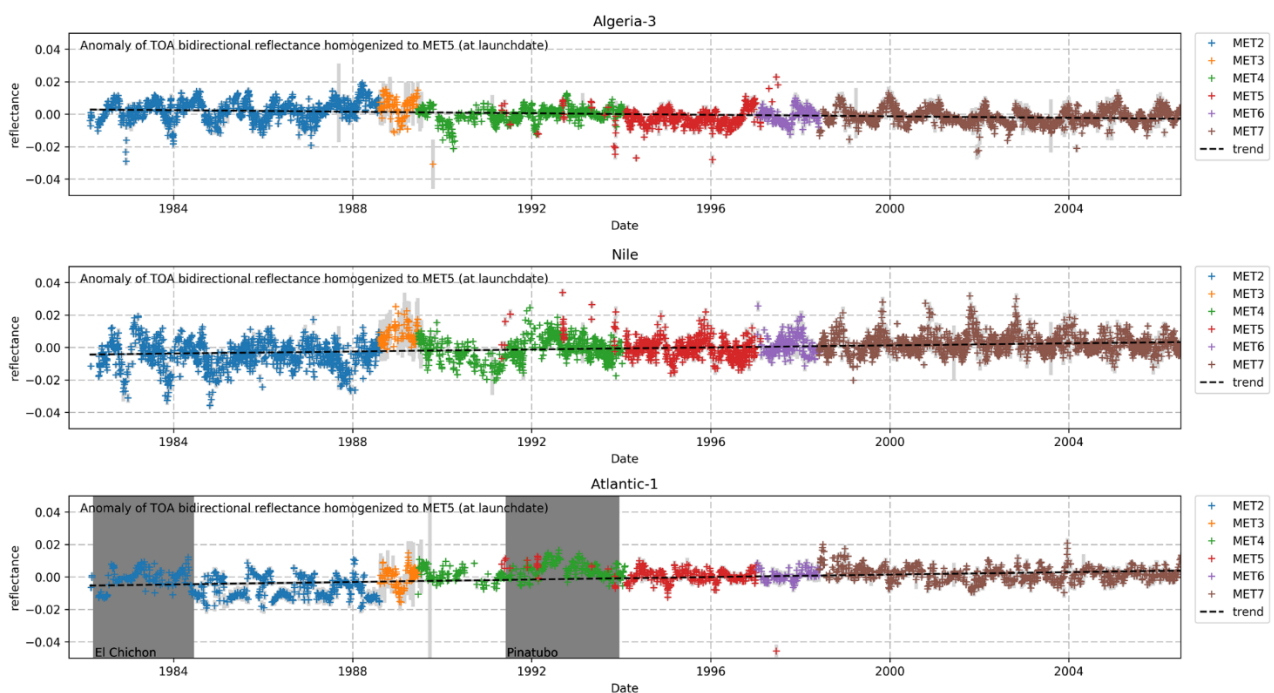


Figure 6: Anomalies of the homogenised clear-sky reflectance time series and their trends at three different sites. Anomalies are the deviation from the mean annual reflectance cycles. Bright grey shading denotes the uncertainties. Additional filtering for cloud contamination was applied as described in the text. Note that for the Atlantic site the periods with globally elevated aerosol loads due to volcanic eruptions (dark grey shading) are excluded from the stability analysis.

Table 4: Stability assessment of the harmonised and homogenised FCDR at three reference sites.

Site	Mean Reflectance	Stability of Reflectance	Relative Stability
		[reflectance decade ⁻¹]	[% decade ⁻¹]
Algeria-3	0.36 ± 0.02	-0.0024 ± 0.000	-0.65 ± 0.02
Nile	0.18 ± 0.03	0.0031 ± 0.000	1.78 ± 0.03
Atlantic-1	0.05 ± 0.00	0.0038 ± 0.000	7.46 ± 0.01

4.1.2 Infra-red and Water vapour channels

Tabata et al., 2019 [RD 16] applied the recalibration methods described in [RD 6] to IR and WV measurements of Japanese geostationary satellites and demonstrated the improvements of recalibrated radiances and better stability in the time series compared to operational radiances. Here we demonstrate the same for the Meteosat IR and WV recalibrated radiances compared to the operational radiances. For this, homogenised radiances are used, that is, radiances spectrally adjusted so that measurements of all instruments look like they are from a common instrument. The common or baseline instrument chosen for the homogenisation is the MVIRI onboard Meteosat-5. Details on the computation of spectral band adjustment factors is described in [RD 1] and [RD 6]. The adjustment factors for all MVIRI instruments are given in Table 5. If the radiances were not homogenised, inter-satellite differences would be visible in the time series due to their different spectral response functions.

Table 5: Spectral band adjustment factors (offset [$mW/m^2/sr/cm^{-1}$] and slope [unit less]) for the IR and WV channels to convert recalibrated radiances to homogenised radiances by taking Meteosat-5 as baseline.

Satellite	Water vapour (WV) channel			Infra-Red (IR) channel		
	offset	slope	uncertainty	offset	slope	uncertainty
Meteosat-2	-0.1647	0.7471	0.1031	-0.1385	0.9944	0.0670
Meteosat-3	-0.1890	0.7111	0.1173	-0.3393	0.9933	0.1187
Meteosat-4	0.0022	0.9428	0.0145	0.0622	0.9976	0.0164
Meteosat-5	0.0000	1.0000	0.0000	0.0000	1.0000	0.0000
Meteosat-6	0.0151	0.9646	0.0120	-0.1422	0.9948	0.0664
Meteosat-7	-0.0887	0.8868	0.0334	-0.7419	0.9930	0.2187

Operational radiances are computed by multiplying the calibration coefficient with a measured count for a IR/WV channel measurement and subtracting the space count. Both calibration coefficients and space counts are available from the following EUMETSAT webpage:

<https://www.eumetsat.int/website/home/Data/Products/Calibration/MFGCalibration/index.html>

This procedure converts measured counts into radiances in $W/m^2/sr$. These radiances are then converted to radiances in $mW/m^2/sr/cm^{-1}$ using the spectral response function of the instrument so that it can be directly compared to the recalibrated radiances (I).

$$L [mWm^{-2}sr^{-1}cm] = L[Wm^{-2}sr^{-1}] \frac{1000}{\int SRF [cm^{-1}]} \quad (1)$$

where $\int SRF$ is the integral of the spectral response function in cm^{-1} .

The unit conversion factors, $1000/\int SRF$, for each channel and instrument and are given in Table 6.

Table 6: Unit conversion factor (1000/filter_integral) to convert radiances from $W/m^2/sr$ to $mW/m^2/sr/cm^{-1}$.

Channel	Meteosat-2	Meteosat-3	Meteosat-4	Meteosat-5	Meteosat-6	Meteosat-7
IR	9.46784	8.14512	9.98144	9.92062	9.56160	7.55977
WV	3.02425	3.15900	4.77034	4.14908	4.72706	3.90292

For the evaluation of the time series, for each time slot, radiances are averaged over the centre of the Meteosat disc, taking pixels 750 to 1750 on both pixel (East-West) and line (North-South) directions. Figure 7 shows the homogenised time series of operational IR channel radiances for the six MFG satellites. One striking feature is the discrepancy for Meteosat-2 and -3 radiances. The differences are presumably arising from a wrong definition of radiance units while deriving the operational calibration coefficients. The calibration coefficients for the two satellites are considerably lower than those of the other satellites. For example, the operational calibration coefficient for Meteosat-2 on 1984-08-15, slot 36 is 0.040587 and for Meteosat-3 on 1988-08-15, slot 18 it is 0.043300, but for Meteosat-4 on 1999-08-17, slot 16, it is 0.078850. A systematic difference in radiance between Meteosat-2 and -3 can also be seen. Some large outliers are also present in the operational time series.

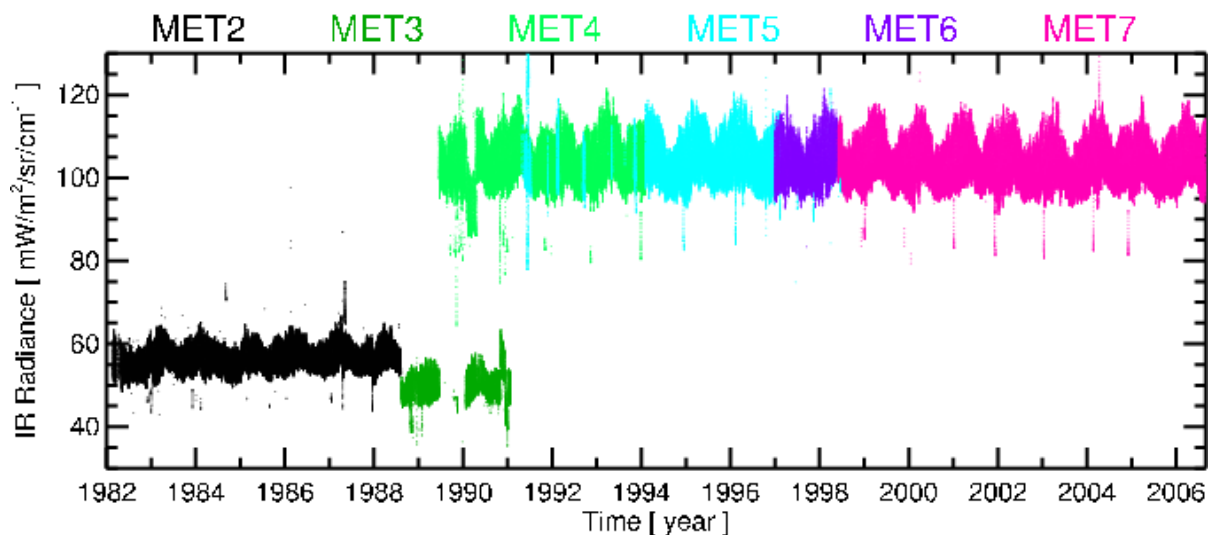


Figure 7: Homogenised time-series of operational IR channel radiances for the 0-degree measurements period. The homogenisation is performed using Meteosat-5 as the baseline satellite. The method to derive spectral band adjustment factors for the homogenisation is described in [RD 1] and [RD 6]. Each data point represents the average radiance of a slot (see text for details).

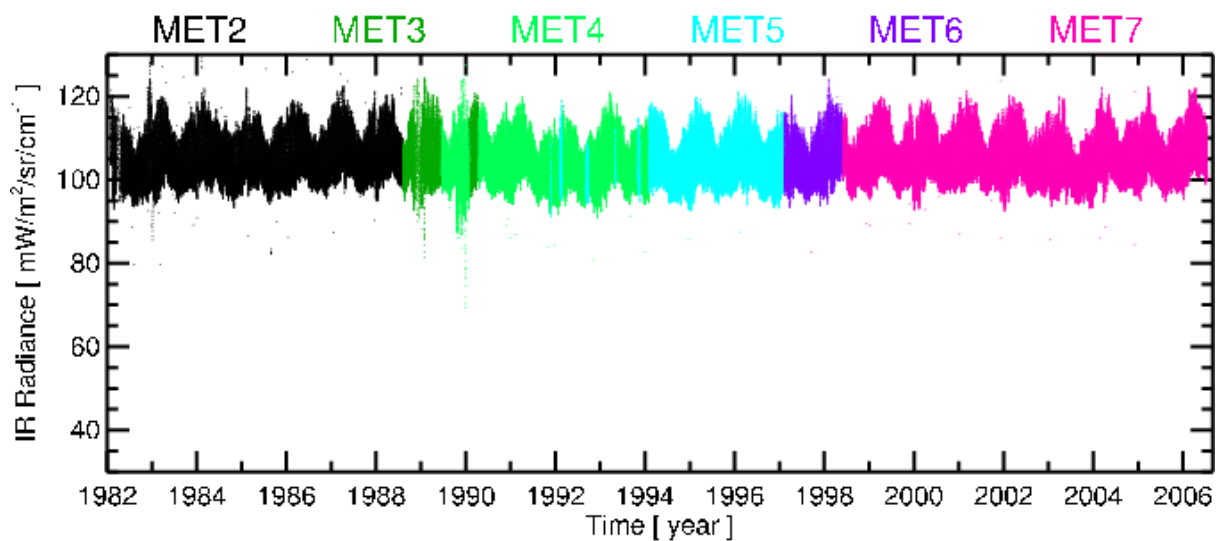


Figure 8: Homogenised time-series of **recalibrated** IR channel radiances for the 0-degree measurements period. The homogenisation is performed using Meteosat-5 as the baseline satellite. The method to derive spectral band adjustment factors for the homogenisation is described in RD 1. Each data point represents the average radiance of a slot (see text for details).

Figure 8 presents homogenised time series of recalibrated radiances. The recalibrated radiances demonstrate a stable time series meaning that there is no evidence of significant inter-satellite differences. The mean, standard deviation, and the long-term trend of the time series are 104.16, 5.19, and 0.11 mW/m²/sr/cm⁻¹/decade. There are also no major outliers seen in the recalibrated time series. Thus, the recalibrated radiances demonstrate a significant improvement over the operational radiances. There are still some outliers present in the recalibrated time series, which may result from the anomalies in the image data which were found in a separate study to detect anomalies in the MFG images [RD 34] but were not known during this processing.

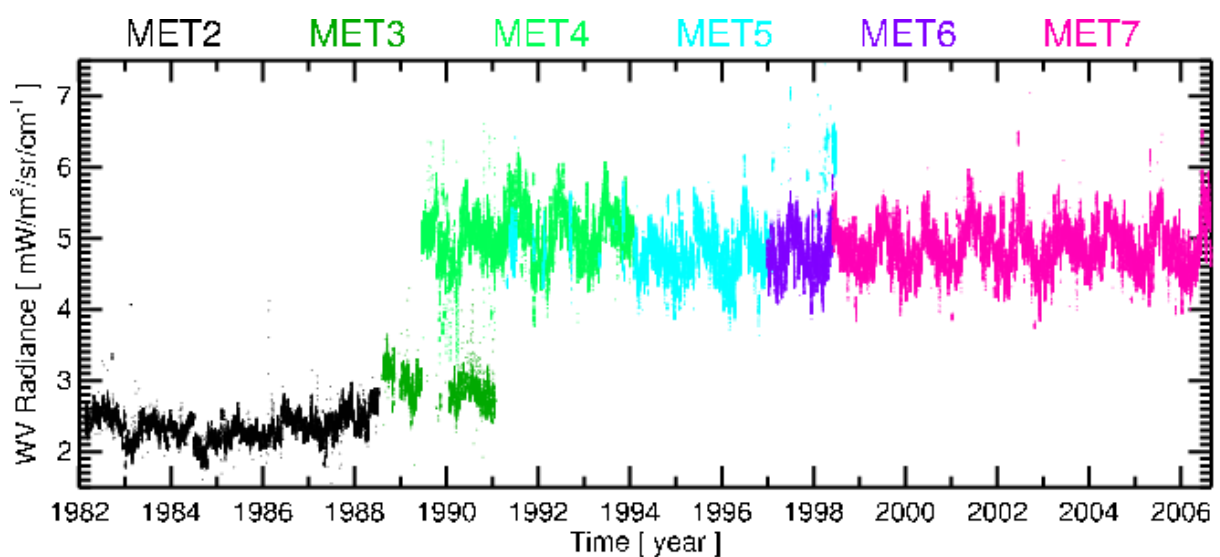


Figure 9: Homogenised time-series of **operational** WV channel radiances for the 0-degree measurements period. The homogenisation is performed using Meteosat-5 as the baseline satellite. The method to derive spectral band

adjustment factors for the homogenisation is described in RD 7. Each data point represents the average radiance of a slot (see text for details).

Similarly, Figure 9 and Figure 10 show homogenised time series of operational and recalibrated WV radiances for the MFG satellites during their 0-degree measurement period. Like in the case of the IR channel, operational radiances of WV channel also show significantly lower radiance values for Meteosat-2 and -3 and there are also some outliers seen in the time series. However, the homogenised recalibrated radiances depict a stable time series. The mean, standard deviation, and the long-term trend of the time series are 4.30, 0.32, and -0.16 mW/m²/sr/cm-1/decade. A few outliers present in the Meteosat-2 and -3 radiances result from the image anomalies as discussed before. Note that for these satellites, the WV channel measurements were recorded in 6-bits compared to the 8-bits data for the other satellites.

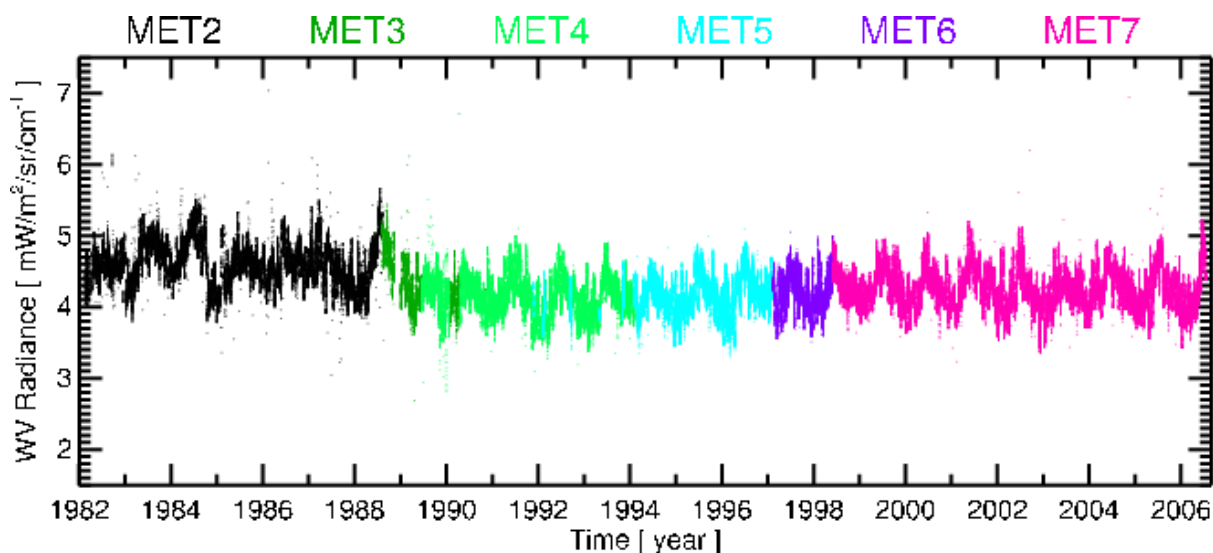


Figure 10: Homogenised time-series of recalibrated WV channel radiances for the 0-degree measurements period. The homogenisation is performed using Meteosat-5 as the baseline satellite. The method to derive spectral band adjustment factors for the homogenisation is described in RD 7. Each data point represents the average radiance of a slot (see text for details).

4.2 Comparison against superior reference

4.2.1 Visible channel

For the validation of the MVIRI VIS band, two superior instruments are available: the HRVIS band of the SEVIRI instrument on Meteosat-8 and the SCIAMACHY instrument on board Envisat. Flying on the second generation of Meteosat satellites, the pre-launch characterisation of the SEVIRI instrument has been significantly improved as compared to MVIRI. As described above, SEVIRI on Meteosat-8 was operated at a sub-satellite point very close to Meteosat-7 during the years 2004-2006. While the SEVIRI HRVIS band covers the same spectral interval as MVIRI VIS, the shapes of the SRFs are different. Thus, in order to compare the two sensors, one instrument has to be band adjusted to the other.

For desert areas, it can be expected that MVIRI's VIS band operational data are comparable to SEVIRI operational data using the original pre-launch SRFs. This is because both instruments use the same desert sites for calibration. For cloudy and sea areas, the original MVIRI's VIS

band operational data is expected to be darker and the recalibrated FCDR is expected to match closer with SEVIRI above sea and cloud targets. SCIAMACHY, on the other hand, is a hyperspectral sensor that allows to evaluate co-locations independently from differing spectral response of the targets. The instrument was operated on a polar orbiter and has very large pixel sizes. Therefore, only few co-located observations with comparable viewing geometries are available [RD 14]. Due to the SRF reconstruction for MVIRI, the recalibrated MVIRI reflectance is expected to match closer with the convoluted reflectance derived from SCIAMACHY measurements.

Comparison against SEVIRI

Rüthrich et al (2019) [RD 9] have described the methods to compare MVIRI VIS reflectance data against SEVIRI HRVIS reflectance data. The MVIRI reflectance is spectrally adjusted to SEVIRI HRVIS channel reflectance before the comparison is made. In the following, three datasets are compared, (i) the operational MVIRI VIS reflectance, (ii) the recalibrated MVIRI VIS reflectance, and (iii) the operational SEVIRI HRVIS reflectance.

For the Algeria-3 desert target, the histograms of clear-sky reflectance from both MVIRI datasets do not deviate much from the histogram of the SEVIRI dataset (Figure 11). Only a subtle bright bias against SEVIRI is observed for both. The good fit at this site is attributed to the fact that the three datasets were all calibrated using desert sites with comparable, red spectral characteristics. While this forces all instruments to measure the same over desert-like sites, a bias is introduced as soon as objects in the Field of View (FoV) have different spectral characteristics, such as clouds and ocean surfaces. This is apparent in the reflectance histograms for cloudy scenes shown in Figure 12. This Figure shows the histograms of fully cloudy pixels with cloud-tops at three different pressure levels (high clouds (above 200 hPa), middle clouds (between 200 hPa and 700 hPa) and low clouds (below 700 hPa)). From the figure, it can be seen that reflectance values across all cloud levels are lower for the operational MVIRI dataset than in the SEVIRI HRVIS dataset. In the histograms of the recalibrated MVIRI reflectance, this dark bias is slightly reduced for low and middle clouds and strongly reduced for high clouds. For high clouds, the observed shift towards brighter cloud reflectance values would affect the top of the atmosphere outgoing shortwave radiation by roughly 8 W/m². Similar behaviour is observed over the Atlantic-1 target. Here the histogram from the operational dataset is also darker than that from the SEVIRI dataset (Figure 13) and the histogram from the recalibrated MVIRI VIS reflectance matches much better with the histogram of the SEVIRI dataset. The better match between the recalibrated data and the SEVIRI dataset is encouraging and confirms that the clear-sky and cloudy reflectance at target sites with different spectral characteristics are better (assuming SEVIRI is the better-characterised instrument) represented when using reconstructed SRFs compared to the use of original (pre-launch) SRFs.

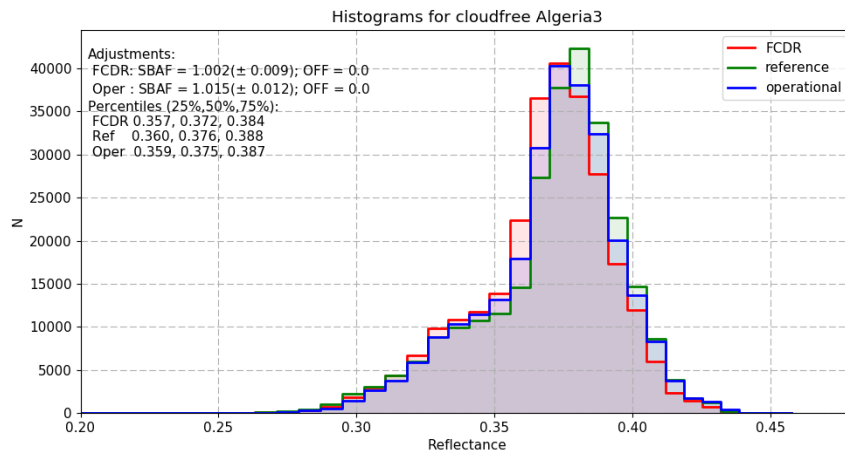


Figure 11: Histogram of SEVIRI HRVIS reflectance plotted as reference together with the histograms of the operational MVIRI reflectance and the recalibrated MVIRI reflectance, as obtained from cloud-free Algeria-3 pixels at 12:00 UTC slots during March 2005. The MVIRI datasets are band adjusted to the SRF of the SEVIRI HRVIS band according to the given Spectral Band Adjustment Factors (SBAFs). The SBAFs are computed using the same set of SCIAMACHY spectra and the difference between both SBAFs is entirely due to the different shapes of the MVIRI SRFs in the operational and the recalibrated datasets.

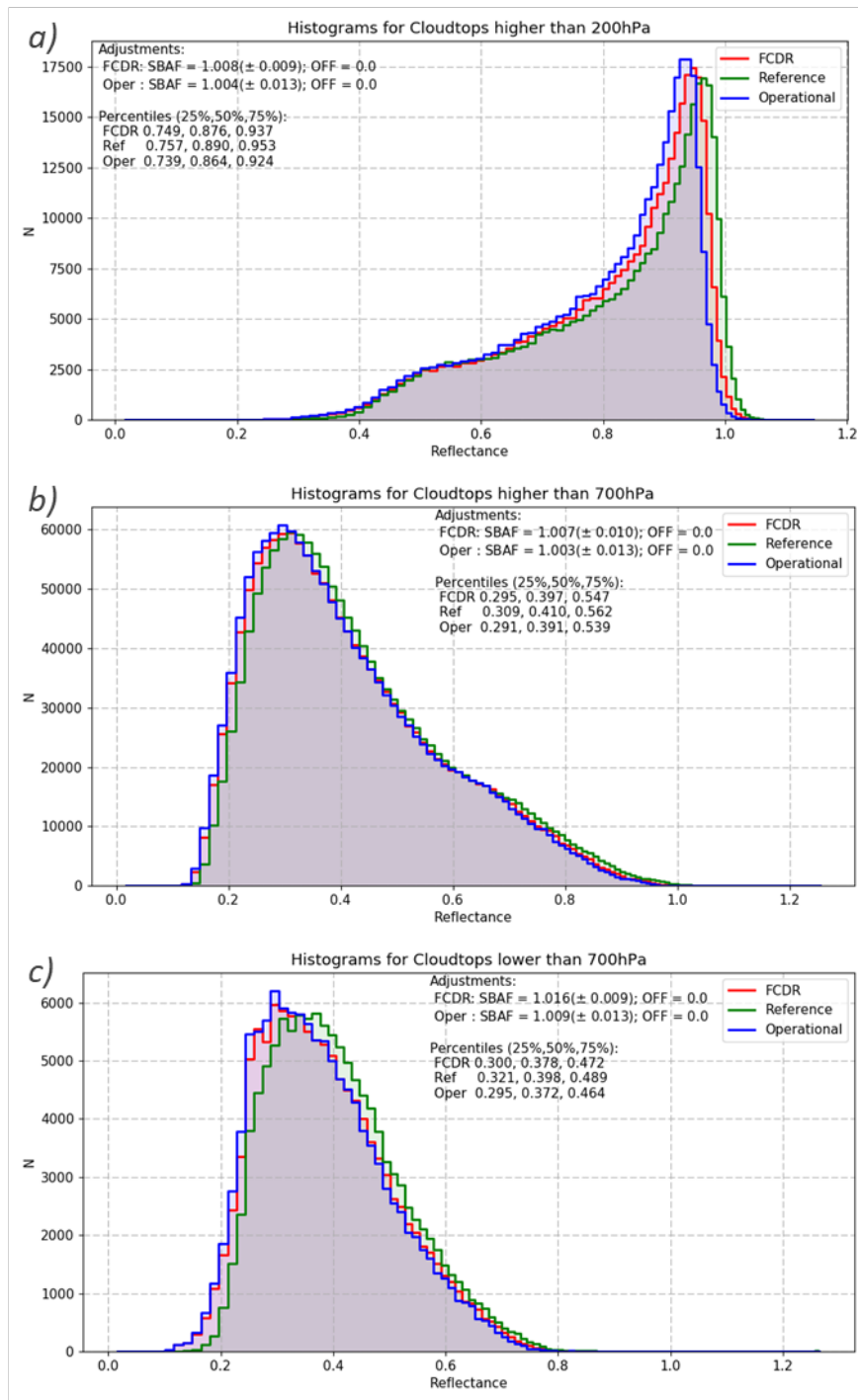


Figure 12: Histogram of SEVIRI HRVIS reflectance plotted as reference together with the histograms of the operational MVIRI reflectance and the recalibrated MVIRI reflectance, as obtained from entirely cloud-covered pixels at 12:00 UTC slots during March 2005. Clouds are classified into high clouds (a), middle clouds (b) and low clouds (c). The MVIRI datasets were band adjusted to the SRF of the SEVIRI HRVIS band according to the given SBAFs. For each cloud-class the SBAFs for the operational dataset and for the recalibrated dataset are computed using the same set of SCIAMACHY spectra and the difference between both SBAFs is entirely due to the different shapes of the SRFs in the operational and recalibrated datasets.

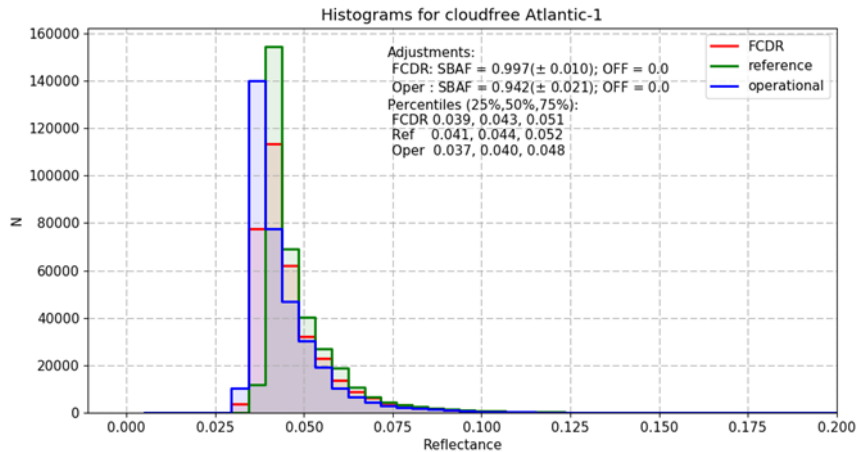


Figure 13: Histogram of SEVIRI HRVIS reflectance plotted as reference together with the histograms of the operational MVIRI reflectance and the recalibrated MVIRI reflectance, as obtained from cloud-free Atlantic-1 pixels at 12:00 UTC slots during March 2005. The MVIRI datasets were band adjusted to the SRF of the SEVIRI HRVIS band according to the given SBAFs. The SBAFs are computed using the same set of SCIAMACHY spectra and the difference between both SBAFs is entirely due to the different shapes of the SRFs in the operational and the recalibrated datasets.

Comparison against SCIAMACHY

SCIAMACHY spectra can be used to simulate the expected reflectance signal of a monitored broadband visible sensor by convoluting the measured reflectance spectrum from SCIAMACHY with the SRF of the monitored sensor. Co-located pairs of SCIAMACHY simulated reflectance and reflectance observed by the monitored instrument can only be compared in case they have similar observing times, viewing conditions and illumination geometries (also referred to as ray-matching conditions). As outlined in [RD 14], such co-located measurements of SCIAMACHY and a geostationary sensor only occur at certain locations relative to the sub-satellite longitude. This is due to SCIAMACHY’s sun-synchronous orbit and its characteristic pattern of azimuth and zenith viewing angles. The locations with potential for ray-matched co-locations between MVIRI and SCIAMACHY are shown in Figure 14 and characterised in Table 7.

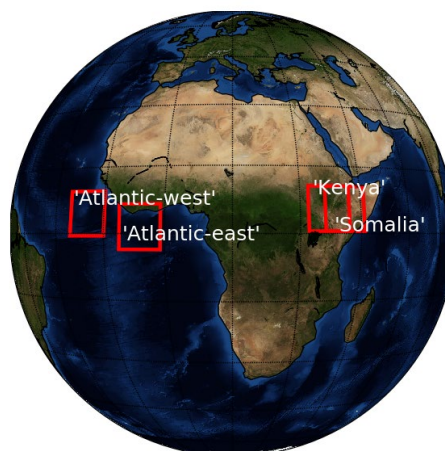


Figure 14: Locations of the areas considered for potentially finding ray-matched SCIAMACHY-MVIRI co-locations with Meteosat data from orbit positions 0° and IODC

Table 7: Geographical coordinates of the areas shown in Figure 14 as well as viewing zenith angle (VZA) and viewing azimuth angle (VAA) of SCIAMACHY observations considered for co-locations.

Location	Central Lat	Central Lon	Surface	Monitored	VZA SCIAM	VAA SCIAM
Atlantic-west	4.5	-20	Sea	MET-7 0°	~26.7	~102.5
Atlantic-east	1.5	-6	Sea	MET-7 0°	~8.8	~102.5
Kenya	5.5	37	Semidesert	MET-7 IODC	~26.7	~102.5
Somalia	5.5	41	Semidesert	MET-5 IODC	~26.7	~102.5

The footprint size and acquisition timespan of SCIAMACHY is variable for the different spectral clusters (Section 3.2.1). The MVIRI SRF spans a very broad domain of the VIS spectrum. In order to be able to convolute the MVIRI SRF with a full SCIAMACHY spectrum, all different spectral clusters of SCIAMACHY need to be integrated to the same footprint size and acquisition timespan. This is done by accumulating the photons at each wavelength over the time interval of the cluster with the longest integration time. As some clusters have very long integration times, only four pixels are available for co-location per scanline. Representative SCIAMACHY spectra from those sites are provided in Figure 15.

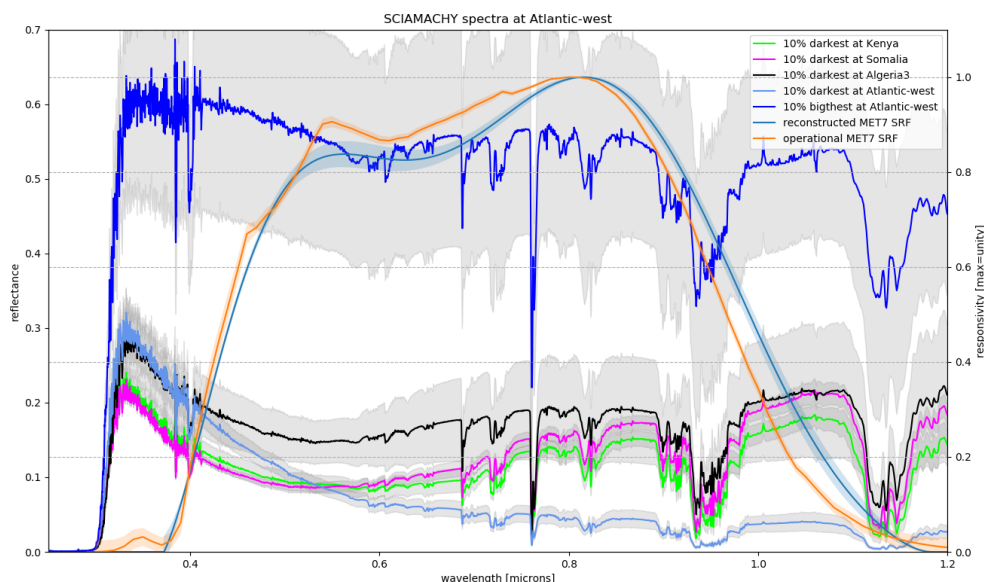


Figure 15: Spectral characteristics of the collocation regions and of Algeria-3 collected during 10 days of February 2005. In order to emphasise on cloud-free surfaces a set of 10% of the darkest spectra was averaged for each region. For the Atlantic site also a set of the 10% brightest spectra was averaged to illustrate the spectral shape of cloudy observations. The grey shading indicates the standard deviation of each set.

The results from the co-locations with SCIAMACHY support the findings from the case-study comparison with SEVIRI. For the semi-arid to arid surfaces of the Kenya and Somalia areas the MVIRI recalibrated reflectance and the operational reflectance have comparable performance (Figure 16, bottom-panels). To understand this, it is necessary to consider the shapes of the spectra at those locations (Figure 15). The spectral shapes of the Kenya and Somalia areas are relatively close to the desert sites that are used for the calibration of both MVIRI datasets (e.g., Algeria-3). Over these two areas the differences between the spectral signatures mainly occur in parts of the spectrum where the original MVIRI SRF does not deviate much from the reconstructed SRF.

This is different for the Atlantic areas where the MVIRI recalibrated reflectance performs significantly better than the operational MVIRI reflectance, with regression slopes improving from about 0.97 for the operational dataset to 0.99 for the MVIRI FCDR. For these areas the

signal of the large SCIAMACHY footprint includes both, blue clear-sky sea spectra and white cloud spectra. An illustration of the spectra is provided in Figure 15 where the 10% darkest Atlantic spectra represent largely cloud-free observations while the 10% brightest Atlantic spectra represent mainly cloudy observations. The combination of dark ocean surfaces with bright clouds explains the large range of the values at the Atlantic areas. The spectral shape of those observations differs strongly from the calibration sites and thus the results are more sensitive to the correction of the degraded SRF. It can be concluded that the use of reconstructed SRFs in the MVIRI FCDR leads to a significant reduction of the dark bias that is observed in the operational MVIRI dataset (Figure 16, top-panels).

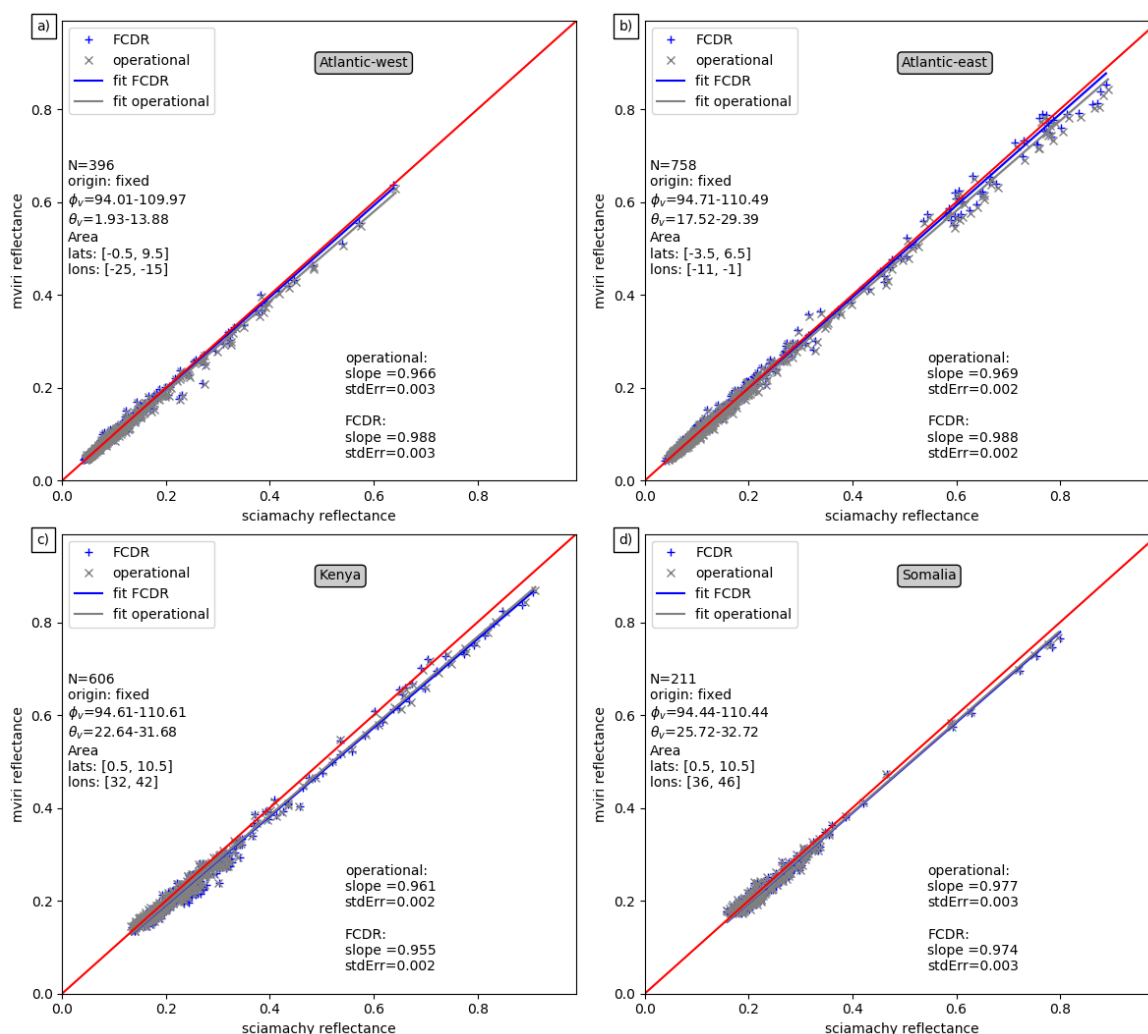


Figure 16: Co-locations between SCIAMACHY and Meteosat-7 MVIRI reflectance for a) Atlantic-west, b) Atlantic-east and c) Kenya. Co-locations between SCIAMACHY and Meteosat-5 MVIRI reflectance are provided in d) for Somalia. Grey marks denote the dataset with the pre-launch SRF characterisation. Blue crosses denote the dataset using the reconstructed SRF. The co-locations are constrained to relative azimuth angles between the two instruments of 5° , to zenith angle differences of 15° and to acquisition time differences of 5 minutes. Only co-locations with a standard deviation of below 0.12 for MVIRI reflectance within a SCIAMACHY pixel are considered in order to reduce the matchup uncertainty for very heterogeneous scenes. Over the Atlantic, areas and the Somalian area co-locations were acquired from data collected during 2002–2006, whereas data collected during 2006–2010 were used for the co-locations over the Kenyan area.

4.2.2 Infra-red and Water vapour channel

The improved quality of the recalibrated radiances was evaluated in four peer-reviewed papers. Firstly, Govaerts et al., 2018 [RD 17] demonstrated improved identification of deep convective clouds by using the recalibrated IR radiances. Secondly, Bojanowski et al., 2018 [RD 18] and Stöckli et al., 2019 [RD 20] used the recalibrated radiances for deriving cloud fractional cover climatology. Finally, Duguay-Tetzlaff et al., 2017 [RD 19] demonstrated the impact of reduced bias and better temporal stability of the recalibrated radiances on a land surface temperature data record. In this report the validity of the recalibrated radiances is further demonstrated in two ways: a) by comparing them to SEVIRI radiances and b) by comparing to GSICS corrected radiances. SEVIRI measurements are considered as superior references compared to MVIRI measurements, but GSICS corrections may not be considered as superior measurements and the comparison against them shall only be considered as a consistency check of the methods as both methods as using IASI as reference measurements.

Comparison against SEVIRI measurements

Meteosat-8, the first satellite in the MSG series was launched in August 2002 carrying the SEVIRI instrument. Since Meteosat-7 was nominally positioned at 0° longitude and Meteosat-8 was nominally positioned at -3.4° longitude, it is possible to compare the measurements of these two instruments. Observations from both instruments were rectified into grids that are centred at 0° longitude. While having the same central longitude, the grids differ in terms of the definition of the geoid. Moreover, the ground pixel resolutions of MVIRI and SEVIRI are different, MVIRI pixels at sub-satellite point has a sampling of $4.5 \times 4.5 \text{ km}^2$ and the SEVIRI pixels at sub-satellite point has a sampling of $3 \times 3 \text{ km}^2$ as shown in Figure 17.

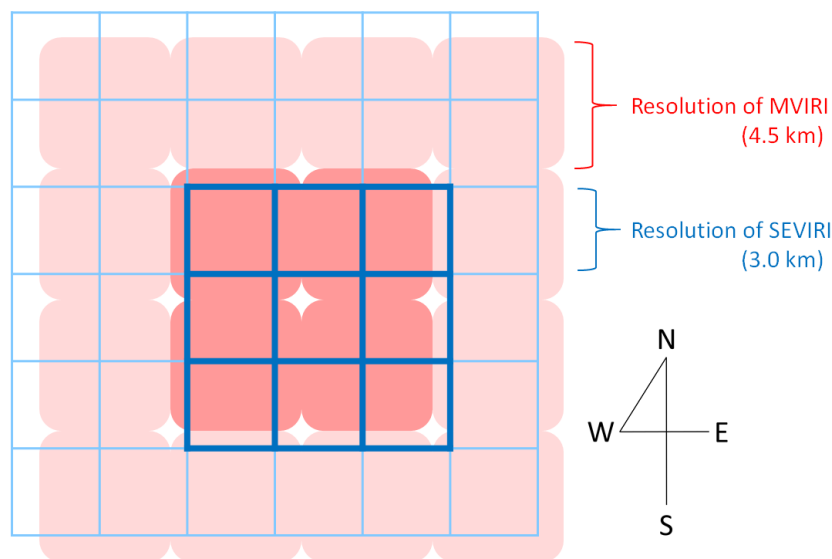


Figure 17: Example schematic (not at the centre of the disc) of the MVIRI (2×2 red boxes) and SEVIRI (3×3 boxes with blue borders) pixel averaging kernels used for the comparison.

In order to have a similar spatial sampling, 2×2 pixels of MVIRI and 3×3 pixels of SEVIRI are averaged before comparing them. The temporal sampling rate of SEVIRI (15min) is double of that of MVIRI (30min), i.e., there are 2 MVIRI images and 4 SEVIRI images per hour. MVIRI imaging starts at 00 and 30 minutes of the hour and it takes about 25 minutes to finish an image. SEVIRI imaging starts at 00, 15, 30 and 45 minutes of the hour and takes about 12.5 minutes to finish an image. Provided that the imaging of both instruments start from the south-east corner of the disc, this implies that the 00 minute image of the MVIRI will have temporal co-

locations with the 00 minute SEVIRI image in the southern hemisphere and with the 15 minute image in the northern hemisphere. Similarly, the 30-minute image of the MIVIRI will have temporal co-locations with the 30-minute SEVIRI image in the southern hemisphere and with the 45-minute image in the northern hemisphere. Only those MVIRI and SEVIRI pixel averages are compared where the centre of the pixel averaging kernels, as shown in Figure 17, are less than 0.5 km apart and the temporal difference is less than 150 seconds. We also used another criterion to constrain the co-locations, which is the product of the distance and time difference to be less than 10 [km sec]. This criterion filtered out those co-locations with large spatial and temporal differences, but allowed to keep those ones with small temporal but with relatively large spatial differences and small spatial but relatively large temporal differences and resulted in much less noise in the comparison results. For the viewing geometry a threshold is defined as function of the viewing zenith angle θ :

$$\Delta\theta = \left| \frac{\cos(\theta_{MVIRI})}{\cos(\theta_{SEVIRI})} - 1 \right| < \theta_{max}, \text{ with } \theta_{max} = 0.03.$$

A MVIRI (Meteosat-7)-SEVIRI (Meteosat-8) comparison is shown in Figure 18. All co-locations satisfying the above-mentioned criteria are further filtered for the scene homogeneity. The 3×3 SEVIRI pixels standard deviation is used as an indicator for the scene homogeneity. The thresholds used for filtering out inhomogeneous scenes are 0.3 and 1.2 $\text{mW/m}^2/\text{sr/cm}^{-1}$ for the WV and IR channels, respectively. Figure 18 shows the 425,561 co-locations found for August 2004 after the filtering. SEVIRI radiances are spectrally adjusted to match MVIRI measurements, the adjustment factors are computed as described in [RD 6]. In Figure 18, the upper panels show results for the IR channel, the lower panels show results for WV channel, left panels show results for operationally calibrated radiances, and the right panels show results for the recalibration radiances. The mean difference between MVIRI and SEVIRI are -1.34 and 0.63 before calibration and 0.73 and 0.03 $\text{mW/m}^2/\text{sr/cm}^{-1}$ after recalibration for the IR and WV channels, respectively, which is a significant improvement in agreement made through recalibration. Note that the standard error of the values are very small due to the large sample size.

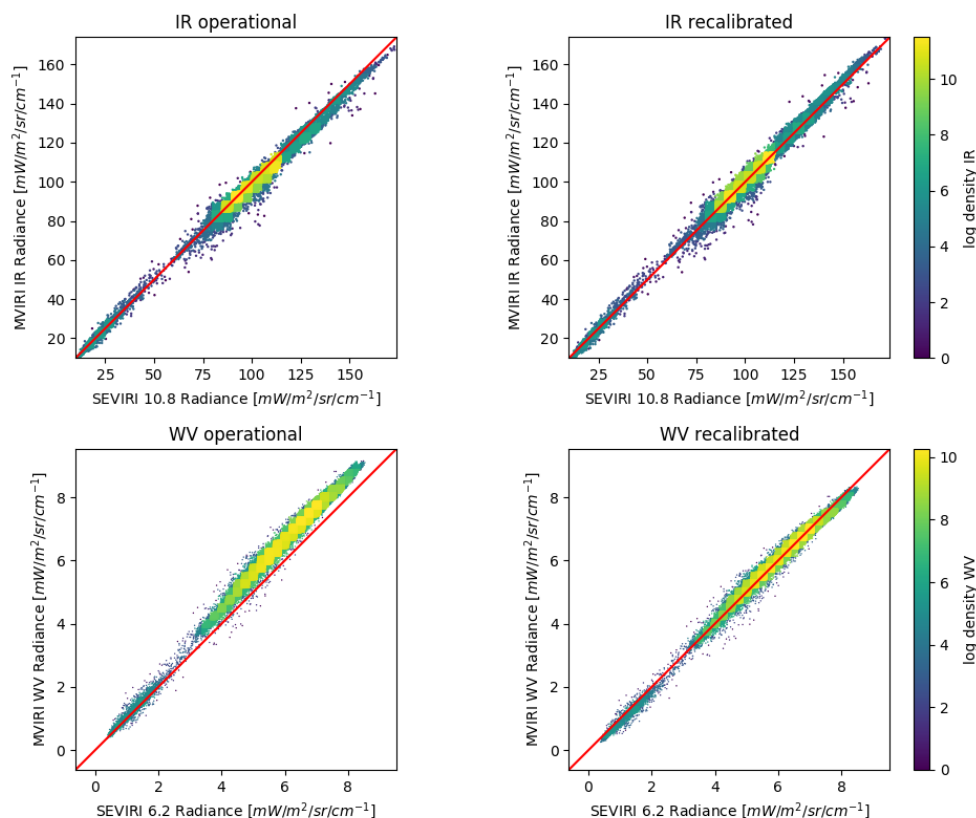


Figure 18: Results of the comparison of Meteosat-7 MVIRI operational (left) and recalibrated (right) against Meteosat-8 SEVIRI operational measurements for August 2004. The SEVIRI measurements are spectrally adjusted to MVIRI measurements as described in Section 4.1.2.

Comparison against GSICS results

Figure 19 shows a comparison between the recalibrated radiances and the corrected radiances based on the method used by GSICS (Note the GSICS correction for MFG is a demonstrational product) for Meteosat-7 during 2015-2016. Both the recalibration coefficients and GSICS corrections were derived based on IASI measurements, but there are some differences in the methods, for example, GSICS uses only night-time overpasses of IASI (this is mainly to avoid solar contamination in the 3.9 micron channel) [RD 21], whereas the recalibration method uses both day and night overpasses. The GSICS correction is based on accumulating collocations for 29 days in the past [RD 21], whereas the recalibration method computes recalibration coefficients based on 5 days of co-locations centred in time around the date for which the calibration is determined. In spite of these differences, it is encouraging to note that both methods give very similar results.

The mean and standard deviation of the operational calibrated, GSICS corrected, and recalibrated time series shown are 92.00 ± 4.61 , 96.46 ± 4.79 , 96.17 ± 4.81 mW/m²/sr/cm⁻¹ for the IR channel and 4.65 ± 0.30 , 4.23 ± 0.28 , and 4.21 ± 0.28 mW/m²/sr/cm⁻¹ for the WV channel, respectively. The relative differences between the operational calibrated and GSICS corrected radiances against our recalibrated radiances are 4.3% and 0.3% for the IR channel and 10.5% and 0.4% for the WV channel. This shows there are significant differences between the operational calibrated radiances and GSICS-corrected or recalibrated radiances. The operational calibrated radiances are colder for the IR channel and warmer for the WV channel.

The close agreement between the GSICS corrected and the recalibrated radiances warrants the validity of our recalibration method.

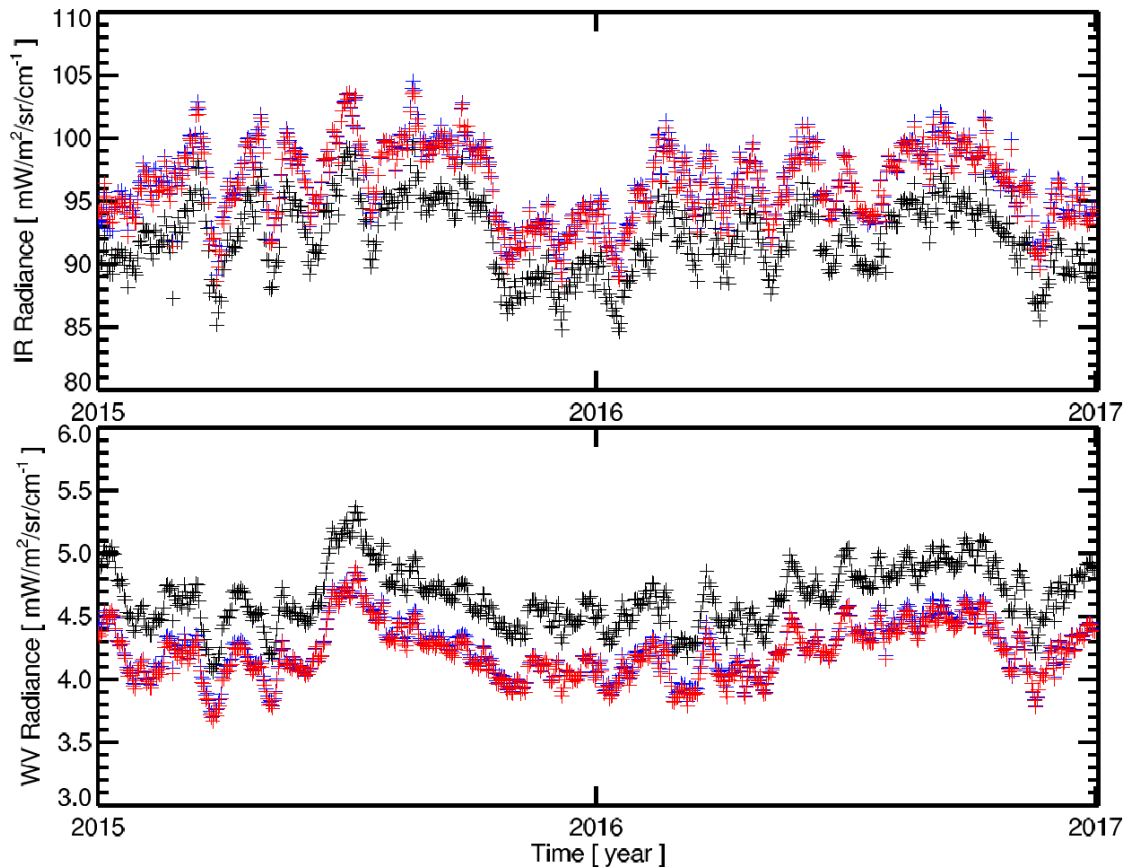


Figure 19: Comparison of operational (black), GSICS corrected (blue), and recalibrated (red) radiances for IR (top) and WV (bottom) channel measurements, see text for details.

5 SUMMARY AND CONCLUSIONS

This report describes the validation results for Release 1 of the FCDR of re-calibrated level-1.5 IR, WV, and VIS radiance from the MVIRI instruments onboard the Meteosat-2, -3, -4, -5, -6, and -7 satellites over the period 1982–2017. The quality of the released FCDR is validated through time-series analysis and by comparing against superior reference observations.

For the IR and WV channel recalibrated radiances, the improvements over the operational calibration has been demonstrated by two comparisons. Firstly, by comparing the MVIRI recalibrated radiances with the GSICS-corrected MVIRI radiances. Secondly, by comparing MVIRI recalibrated radiances with SEVIRI radiances. Both comparisons show the recalibration could correct for radiometric anomalies in the operational radiances. Compared to the operational radiances, significant reduction in biases were observed for both IR and WV channels, of 4% and 10%, respectively. The mean absolute difference between recalibrated radiances and SEVIRI radiances are 0.73 and 0.03 $\text{mW/m}^2/\text{sr/cm}^{-1}$ for the IR and WV channels, respectively, which corresponds to differences of less than 1%. These values are significantly smaller than the differences between operational calibrated radiances and recalibrated radiances. Further, the recalibrated radiances had already been used in several applications [RD

17], [RD 18], [RD 19] and [RD 20] that showed their superiority to operational calibrated radiances. The recalibration, therefore, successfully eliminates the jump between the time series of MVIRI and SEVIRI measurements.

For the VIS band, a thorough validation against data from the HRVIS channel of the SEVIRI instrument onboard Meteosat-8 and against co-located and ray-matched measurements from SCIAMACHY that served as reference, the improved reflectance over cloudy and ocean areas in the new FCDR was demonstrated. Over cloudy areas, the harmonised MVIRI FCDR is brighter than the operational MVIRI data record, which results in a better match with the SEVIRI cloud reflectance. The brighter reflectance values for high-clouds, for example, are estimated to affect the top of atmosphere outgoing shortwave radiation by about 8 W/m^2 . The difference between the harmonised MVIRI FCDR and the operational MVIRI data record is small over areas with dominant spectral contributions in the green and red part of the spectrum.

The comparison to SCIAMACHY data has confirmed the findings from the comparison against the SEVIRI data, which indicates the robustness of the validation results. The analysis of co-locations between the harmonised MVIRI FCDR and SCIAMACHY has revealed excellent agreement with slopes close to unity (~ 0.98 over ocean areas and ~ 0.96 over land areas). It is concluded that the use of reconstructed SRFs in the MVIRI FCDR leads to a significant reduction of the dark bias that is observed in the operational MVIRI dataset.

6 REFERENCES

<i>Number</i>	<i>Document Name</i>	<i>Reference</i>
RD 1.	Algorithm Theoretical Baseline Document – MVIRI FCDR Release 1, EUM/OPS/DOC/18/990143	
RD 2.	Product User Guide - MVIRI FCDR Release 1, EUM/USC/DOC/17/906121	
RD 3.	ERA-CLIM2 European Union’s Seventh Framework Programme (FP7; Grant Agreement No. 607029 (2014). http://cordis.europa.eu/project/rcn/188832_en.html (accessed on 6 December 2018)	
RD 4.	FIDUCEO project description. www.fiduceo.eu (accessed on 6 December 2018)	
RD 5.	GCOS-154, 2011: Systematic Observation Requirements for Satellite-Based Products for Climate, 2011 Update, December 2011, 139 pp.	
RD 6.	John, V.O.; Tabata, T.; R��thrich, F.; Roebeling, R.; Hewison, T.; St��ckli, R.; Schulz, J. On the Methods for Recalibrating Geostationary Longwave Channels Using Polar Orbiting Infrared Sounders. <i>Remote Sens.</i> 2019, 11, 1171.	
RD 7.	Govaerts, Y.; R��thrich, F.; John, V.; Quast, R. Climate Data Records from Meteosat First Generation Part I: Simulation of Accurate Top-Of-Atmosphere Spectral Radiance over Pseudo-Invariant Calibration Sites for the Retrieval of the in-flight MVIRI/VIS Spectral Response. <i>Remote Sens.</i> 2018, 10, 1959, doi:10.3390/rs10121959.	
RD 8.	Quast, R.; Giering, R.; Govaerts, Y.; R��thrich, F.; Roebeling, R. Climate Data Records from Meteosat First Generation Part II: Retrieval of the In-Flight VIS Spectral Response. <i>Remote Sens.</i> 2019, 11, 480, doi:10.3390/rs11050480.	
RD 9.	R��thrich, F.; John, V.O.; Roebeling, R.A.; Quast, R.; Govaerts, Y.; Wooliams, E.; Schulz, J. Climate Data Records from Meteosat First Generation Part III: Recalibration and Uncertainty Tracing of the Visible Channel on Meteosat-2–7 Using Reconstructed, Spectrally Changing Response Functions. <i>Remote Sens.</i> 2019, 11, 1165.	
RD 10.	SEVIRI Solar Channel Calibration: Algorithm Specification Document, EUM/MSG/SPE/411	
RD 11.	Decoster, I.; Govaerts, Y.M.; Baudrez, E.; Dewitte, S.; Velazquez, A.; Blazquez, A.; Cornelis, J. Evidence of pre-launch characterization problem of Meteosat-7 visible spectral response. <i>Remote Sensing Letters</i> 2013, 4, 1008–1017. doi:10.1080/2150704X.2013.828181.	
RD 12.	Govaerts, Y. M. Correction of the Meteosat-5 and -6 radiometer solar channel spectral response with the Meteosat-7 sensor spectral characteristics. <i>International Journal on Remote Sensing</i> 1999, 10 (18), 3677-3682. Doi: 10.1080/014311699211273	
RD 13.	Decoster, I.; Clerbaux, N.; Baudrez, E.; Dewitte, S.; Ipe, A.; Nevens, S.; Blazquez, A.; Cornelis, J. Spectral Aging Model Applied to Meteosat First Generation Visible Band. <i>Remote Sensing</i> 2014, 6, 2534-2571. doi: 10.3390/rs6032534.	
RD 14.	Doelling, D., Scarino, B., Morstad, D., Gopalan, A., Bhatt, R., Lukashin, C. and Minnis, P. The Intercalibration of Geostationary Visible Imagers Using Operational Hyperspectral SCIAMACHY Radiances. <i>IEEE Transactions on Geoscience and Remote Sensing</i> 2013, 10 (3).	
RD 15.	Goldberg, M., G. Ohring, J. Butler, C. Cao, R. Datla, D. Doelling, V. Gaertner, T. Hewison, B. Iacovazzi, D. Kim, T. Kurino, J. Lafeuille, P. Minnis, D. Renaut, J. Schmetz, D. Tobin, L. Wang, F. Weng, X. Wu, F. Yu, P. Zhang, and T. Zhu, “The global space-based inter-calibration system (GSICS),” <i>Bull. Amer. Meteorol. Soc.</i> , vol. 92, no. 4, pp. 468–475, Apr. 2011.	
RD 16.	Tabata, T.; John, V.O.; Roebeling, R.A.; Hewison, T.; Schulz, J. Recalibration of over 35 Years of Infrared and Water Vapor Channel Radiances of the JMA Geostationary Satellites. <i>Remote Sens.</i> 2019, 11, 1189.	
RD 17.	Govaerts, Y.M.; R��thrich, F.; John, V.O.; Quast, R. Climate Data Records from Meteosat First Generation Part I: Simulation of Accurate Top-of-Atmosphere Spectral Radiance over Pseudo-	

	Invariant Calibration Sites for the Retrieval of the In-Flight Visible Spectral Response. <i>Remote Sens.</i> 2018, 10, 1959.
RD 18.	Bojanowski, J.S.; Stöckli, R.; Duguay-Tetzlaff, A.; Finkensieper, S.; Hollmann, R. Performance Assessment of the COMET Cloud Fractional Cover Climatology across Meteosat Generations. <i>Remote Sens.</i> 2018, 10, 804.
RD 19.	Duguay-Tetzlaff, Anke; Stöckli, Reto; Bojanowski, Jędrzej; Hollmann, Rainer; Fuchs, Petra; Werscheck, Martin (2017): CM SAF Land Surface Temperature dataset from METeosat First and Second Generation - Edition 1 (SUMET Ed. 1), Satellite Application Facility on Climate Monitoring, DOI:10.5676/EUM_SAF_CM/LST_METEOSAT/V001, https://doi.org/10.5676/EUM_SAF_CM/LST_METEOSAT/V001
RD 20.	Stöckli, R.; Bojanowski, J.S.; John, V.O.; Duguay-Tetzlaff, A.; Bourgeois, Q.; Schulz, J.; Hollmann, R. Cloud Detection with Historical Geostationary Satellite Sensors for Climate Applications. <i>Remote Sens.</i> 2019, 11, 1052.
RD 21.	Hewison, T. J., X. Wu, F. Yu, Y. Tahara, X. Hu, D. Kim and M. Koenig, 2013: GSICS Inter-Calibration of Infrared Channels of Geostationary Imagers using Metop/IASI, <i>IEEE Trans. Geosci. Remote Sens.</i> , vol. 51, no. 3, doi:10.1109/TGRS.2013.2238544.
RD 22.	SCIAMACHY Product Handbook. 2013. Available online: https://earth.esa.int/web/guest/missions/esa-operational-eo-missions/envisat/instruments/sciamachy-handbook/wiki (accessed on 31 January 2019).
RD 23.	Tilstra, L.G.; Tuinder, O.N.E.; Wang, P.; Stammes, P. Surface reflectivity climatologies from UV to NIR determined from Earth observations by GOME-2 and SCIAMACHY. <i>J. Geophys. Res. Atmos.</i> 2017, 122, 4084–4111, doi:10.1002/2016JD025940.
RD 24.	Burrows, J.P.; Goede, A.P.H.; Muller, C.; Bovensmann, H. SCIAMACHY—The Need for Atmospheric Research from Space. In <i>SCIAMACHY-Exploring the Changing Earth's Atmosphere</i> ; Gottwaldand, M., Bovensmann, H., Eds.; Springer, Dordrecht 2011; doi: 10.1007/978-90-481-9896-2_1.
RD 25.	Doelling, D.R.; Lukashin, C.; Minnis, P.; Scarino, B.; Morstad, D. Spectral reflectance corrections for satellite intercalibrations using SCIAMACHY data. <i>IEEE Geosci. Remote Sens. Lett.</i> 2012, 9, 119–123.
RD 26.	Doelling, D.R.; Haney, C.O.; Scarino, B.R.; Gopalan, A.; Bhatt, R. Improvements to the geostationary visible imager ray-matching calibration algorithm for CERES Edition 4. <i>J. Atmos. Ocean. Technol.</i> 2016, 33, 2679–2698.
RD 27.	Roebeling, R.A.; Feijt, A.J.; Stammes, P. Cloud property retrievals for climate monitoring: Implications of differences between Spinning Enhanced Visible and Infrared Imager (SEVIRI) on METEOSAT-8 and Advanced Very High Resolution Radiometer (AVHRR) on NOAA-17. <i>J. Geophys. Res.</i> 2006, 111, D20210, doi:10.1029/2005JD006990.
RD 28.	Musial, J.P.; Bojanowski, J.S. AVHRR LAC satellite cloud climatology over Central Europe derived by the Vectorized Earth Observation Retrieval (VEOR) method and PyLAC software. <i>Geoinf. Issues</i> 2017, 9, 39–51.
RD 29.	Lichtenberg, G.; Kleipool, Q.; Krijger, J.M.; van Soest, G.; van Hees, R.; Tilstra, L.G.; Acarreta, J.R.; Aben, I.; Ahlers, B.; Bovensmann, H.; et al. SCIAMACHY Level 1 data: Calibration concept and in-flight calibration, <i>Atmos. Chem. Phys.</i> 2006, 6, 5347–5367, doi:10.5194/acp-6-5347-2006.
RD 30.	Snel, R.; Lichtenberg, G.; Noël, S.; Krijger, M.; Slijkhuis, K.; Bramstedt, K. Calibration and Monitoring. In <i>SCIAMACHY-Exploring the Changing Earth's Atmosphere</i> ; Gottwaldand, M., Bovensmann, H., Eds.; Springer, Dordrecht 2011; doi: 10.1007/978-90-481-9896-2_5.
RD 31.	SCIAMACHY L1c Command-line Tool Landing Pages. Available online: https://earth.esa.int/web/guest/software-tools/content/-/article/scial1c-command-line-tool-4073 (accessed on 1 February 2019).
RD 32.	Govaerts, Y.; Clerici, M. MSG-1/SEVIRI Solar Channels Calibration Commissioning Activity Report. 2004. Available online: https://www.eumetsat.int/website/home/Data/Products/Calibration/MSGCalibration (accessed on 31 January 2019).

RD 33.	Rüthrich, F.; John, V.O.; Roebeling, R.; Wagner, S.; Viticchie, B.; Hewison, T.; Govaerts, Y.; Quast, R.; Giering, R.; Schulz, J. A Fundamental Climate Data Record that accounts for Meteosat First Generation Visible Band Spectral Response Issues. In Proceedings of the 2016 EUMETSAT Meteorological Satellite Conference, Darmstadt, Germany, 26–30 September 2016.
RD 34.	Liefhebber, F., S. Lammens, P. Brussee, A. Bos, V. O. John, F. Rüthrich, J. Onderwaater, M. G. Grant, and J. Schulz (submitted 2019) Detection of image anomalies in the Meteosat First Generation measurements, Atmospheric Measurement Techniques.
RD 35.	Stöckli, R.; Bojanowski, J.S.; John, V.O.; Duguay-Tetzlaff, A.; Bourgeois, Q.; Schulz, J.; Hollmann, R. Cloud Detection with Historical Geostationary Satellite Sensors for Climate Applications. Remote Sens. 2019, 11, 1052.